Order Number 1345615

Ratioing radiometer, solar diffuser system for in-flight calibration of multispectral satellite sensors

Guzman, Carmen Theresa, M.S.

The University of Arizona, 1991

U·M·I
300 N. Zeeb Rd.
Ann Arbor, MI 48106

RATIOING RADIOMETER, SOLAR DIFFUSER SYSTEM FOR IN-FLIGHT CALIBRATION OF MULTISPECTRAL SATELLITE SENSORS

by

Carmen Theresa Guzman

A Thesis submitted to the Faculty of the

COMMITTEE ON OPTICAL SCIENCES (Graduate)

In Partial Fulfillment of the Requirements

For the Degree of

MASTER OF SCIENCE

In the Graduate College

THE UNIVERSITY OF ARIZONA

1991

STATEMENT BY AUTHOR

This thesis had been submitted in partial fulfillment of requirements for an advanced degree at The University of Arizona and is deposited in the University Library to be made available to borrowers under rules of the Library.

Brief quotations from this thesis are allowable without special permission, provided that accurate acknowledgement of source is made. Requests for permission for extended quotation from or reproduction of this manuscript in whole or in part may be granted by the head of the major department or the Dean of the Graduate College when in his or her judgement the proposed use of the material is in the interest of scholarship. In all other instances, however, permission must be obtained from the author.

SIGNED: Carmen Hussman

APPROVAL BY THESIS DIRECTOR

This thesis has been approved on the date shown below:

P. N. Slater
Professor of Optical Sciences

July 29, 1991
Date

ACKNOWLEDGEMENTS

There are many people the author would like to take the opportunity to thank, because their assistance made this work possible. I would like to thank Dr. Philip N. Slater for allowing me do this thesis and for putting up with all the hassle I caused. I would also like to thank the other group members for their support and help, Dr. Stuart F. Biggar, David I. Gellman, Nianzeng Che, Mark W. Smith, David E. Flittner, Barbara Grant, Quinn Hart, Iain R. Penny and Carter Grotbeck. I would like to thank Wendy Rosenblum (Rochester Institute of Technology) for starting this project and leaving the equipment with notes. I would like to thank Sheryl A. Recker for helping me out and being my mother away from home.

Additionally, I would like to thank the suppliers of the diffuser sample materials, without whom the second half of this thesis would never have been. The samples were donated by Labsphere, J. J. Hsia (NIST), J. M. Palmer, F. J. Gray Co., GTE Wesgo, Erie Ceramic Arts Co., and Y. Harada (IITRI).

The author wishes to thank everybody involved at JPL including Carol J. Bruegge, Edward A. Miller, B. E. Anspaugh and S. B. Gabriel. The work was funded under work order 407224 from the Jet Propulsion Laboratory for HIRIS.

The author would like to thank M. R. Gilmore (TRW) and A. P. Rice (California Institute of Technology) for their assistance in the irradiation work at their respective facilities. The author would like to thank Shahida Rana and Michael Jacobson for the help in taking some of the data.

Most of all, I would like to thank my parents for the steady reminder that I can do whatever I want and nothing can stop me.

TABLE OF CONTENTS

LIST OF ILLUSTRATIONS

LIST OF ILLUSTRATIONS, CONTINUED

LIST OF ILLUSTRATIONS, CONTINUED

LIST OF ILLUSTRATIONS, CONTINUED

LIST OF TABLES

ABSTRACT

One promising way to calibrate a satellite sensor in flight is to place a sun-illuminated white diffuser panel in front of it. However, even if the panel is only deployed for brief periods, it may degrade in the space environment. A ratioing radiometer to monitor the panel changes is described and an error analysis associated with the use of the radiometer is presented.

The procedures used to test the optical properties of different candidate panel materials are described. Results of spectral directional-hemispherical reflectance, bidirectional reflectance, polarization and depolarization measurements are presented for nine panel candidate materials before and after exposure to proton and ultraviolet radiation.

In this preliminary evaluation it was found that, although polytetrafluoroethylene materials exhibited the most desirable characteristics before proton and UV irradiation, IITRI paint YB-71 withstood proton and UV irradiation the best and is the choice among the nine materials tested.

CHAPTER I

INTRODUCTION

The in-flight absolute calibration of multispectral imaging sensors is a problem that has invited many solutions over the years. The Thematic Mapper employed an internal lamp to irradiate the focal plane, Engel and Weinstein 1982. In the case of the Systeme Probatorie d'Observation de la Terre, Haute Resolution Visible, a solar-illuminated fiber optics array and a lamp are used, Begni, et al. 1986. A third method makes use of ground reflectance and atmospheric measurements as inputs to a radiative transfer code that predicts the radiance at the sensor, Slater, et al. 1987.

An alternate approach under consideration for several Earth Observing System (Eos) sensors makes use of an on-board solar diffuser panel that fills the aperture and field-of-view (FOV) of the sensor, thus providing end-to-end sensor calibration. At a certain point in the orbit, this panel is moved to a position where, when viewed by the sensor, it is illuminated by direct sunlight at a known incidence angle. If the directional reflectance characteristics of the panel are known and stable and only direct sunlight is incident on it, the panel provides the required known radiance input to the system for calibration purposes. However, the panel is subject to deterioration due to environmental contamination from outgassed spacecraft materials condensing on it, intense ultraviolet solar irradiance, and erosion by atomic oxygen. Even if the panel is carefully stowed during periods of non-use, the limited exposure may result in changes, and the magnitude of these changes will be unknown. In addition, light may be reflected or scattered onto the panel from other surfaces on the polar platform. If these effects are not monitored, erroneous calibration values will result.

One way out of the dilemma is to use a separate multiband radiometer that can look directly at the sun and the diffuser panel at the same time that the sensor views the panel for calibration. The radiometer need not be extremely stable or carefully calibrated, but it must have sufficient linearity over a wide dynamic range to give meaningful results. This method presumes that the sun is sufficiently stable to be used as the reference calibration source. The Ratioing Radiometer (RR) simply determines the radiance of the diffuser panel with reference to the solar irradiance at the entrance pupil of the radiometer. The sensor is then calibrated with the known panel radiance. Unfortunately, if a simple, single-lens, narrow field, radiometer is used to image the sun and panel, the ratio of outputs will be greater than 10^4. However, a two-lens system is able to decrease this ratio to about 25 which substantially reduces the range over which a radiometer linear response is necessary.

Chapter II of this thesis discusses the design and proof-of-concept of the diffuser panel and ratioing radiometer. This chapter discusses alternative operational modes for the RR-diffuser system, describes the basic design of the RR, and includes radiometric analyses that derive the measured ratio in terms of system parameters. A description of the construction and characterization of a model radiometer is provided. This chapter also presents an error analysis for the calibration of a multispectral satellite sensor using the RR and the diffuser panel with and without stray radiation present.

Chapter III discusses the selection of a diffuser panel that will not degrade significantly in the space environment. There are many factors in space that can cause degradation, as previously mentioned. The characteristics that the diffuser panel should retain are listed. A description of the different materials considered in the selection process are detailed. This chapter describes the test procedure used for evaluating how well diffuser panel materials withstand proton exposure and ultra-violet irradiation. The final section analyzes the test results.

Chapter IV summarizes the conclusions from the material presented in chapters II and III of this thesis.

It should be noted that only the optical degradation of the diffuser panel material in the space environment (solar radiation, local spacecraft contamination, and particles in space, such as protons and atomic oxygen) is discussed in this thesis; before a final selection, thermal and mechanical properties (e.g., hardness, thermal expansion, ease of mounting) must also be taken into consideration.

CHAPTER II

DESIGN OF THE RATIOING RADIOMETER

Section 2.1 of this chapter discusses the operational modes of the panel when stray light is and is not present on the panel, the basic design for the Ratioing Radiometer (RR), and radiometric analyses for the basic RR design. Section 2.2 describes the construction and characterization of a model radiometer built from the basic RR design. Section 2.3 presents an error analysis for the calibration, using a diffuser panel and RR, of a multispectral satellite sensor with and without stray radiation present and with and without panel luminescence.

SECTION 2.1: RATIOING RADIOMETER ANALYSIS

ALTERNATIVE OPERATIONAL MODES

The RR can be used in two different ways in orbit which depend on whether or not it is assumed that the diffuser panel is likely to be irradiated by stray light as well as direct sunlight.

CASE I - No stray light on the panel.

In this case, the panel radiance can be calculated from the knowledge of the exoatmospheric solar irradiance, the BRDF of the panel, and the angle of incidence on the panel. A change in the panel reflectance is detected by a change in the ratio of panel to sun signals. The assumptions are:

(i) The panel does not change in reflectance from its preflight value during the first calibration in orbit. Subsequent calibrations are all done with respect to this calibration. A result of this assumption is that no preflight determination of the ratio is needed (only the reflectance of the panel is measured).

(ii) Stray light must not enter the field of view of the radiometer when it observes the sun and the panel.

(iii) During the lifetime of the sensor, either the loss in reflectance of the panel is not accompanied by a change in the shape of its BRDF, or the angles of incidence of the RR and multispectral satellite sensor at the panel are equal.

In the case where we cannot assume the panel reflectance is unchanged during the first calibration, the ratio of the sun signal to panel signal must be determined by a preflight calibration. A change in this ratio would indicate a change in the reflectance of the panel.

CASE II - With stray light on the panel.

In this case, although the change in radiance of the panel is monitored by the RR, the irradiance on the panel is unknown and, therefore, the radiance of the panel cannot be calculated as in Case I. Consequently an accurate knowledge of the angle of incidence on the panel is of no value; however, a knowledge of the angle will provide a no-stray-light lower bound for the panel radiance. The procedure is to determine the ratio of sun signal to panel signal accurately preflight so that the radiance of the panel is known in terms of the ratio for in-flight calibration purposes. The assumptions are:

(i) Stray light must not enter the field of view of the radiometer when it observes the sun and the panel.

(ii) During the lifetime of the sensor, either the loss in reflectance of the panel is not accompanied by a change in the shape of its BRDF, or the angles of incidence of the RR and multispectral satellite sensor at the panel are equal.

Further thought is needed to determine whether the preflight determination of the ratio can best be done in the laboratory using standard lamps or on the top of a mountain using the sun as source. In the latter case the diffuse component of irradiance on the panel must be accounted for (see the later discussion of results). Ideally, it would be preferable to simulate the complete in-flight calibration procedure. This would mean making a mountain-top calibration of the sensor surrounded by a mock-up of the reflecting surfaces on the polar platform.

DESIGN OF RATIOING RADIOMETER

If a simple radiometer with a detector located at the focus of an objective lens is used, the signal from the direct sun is some 10^4 higher than the signal from a diffuse white panel under solar irradiation because the area of the panel as seen by the radiometer is small and the irradiance of the sun for a direct view is very large. This ratio places stringent demands on the dynamic range and linearity of the detector. By adding a field stop and lens to the simple radiometer, the ratio can be reduced to a reasonable level. The layout is based on a microscope condenser design by Köhler (Born and Wolf, 1983), used to produce a large, uniformly irradiated area from a small source. The field lens, located at the rear focal point of the objective lens, images the uniformly irradiated objective lens onto the focal plane, as shown in Figure 2.1. The focal plane contains filtered detectors or the entrance slit of a spectrometer.

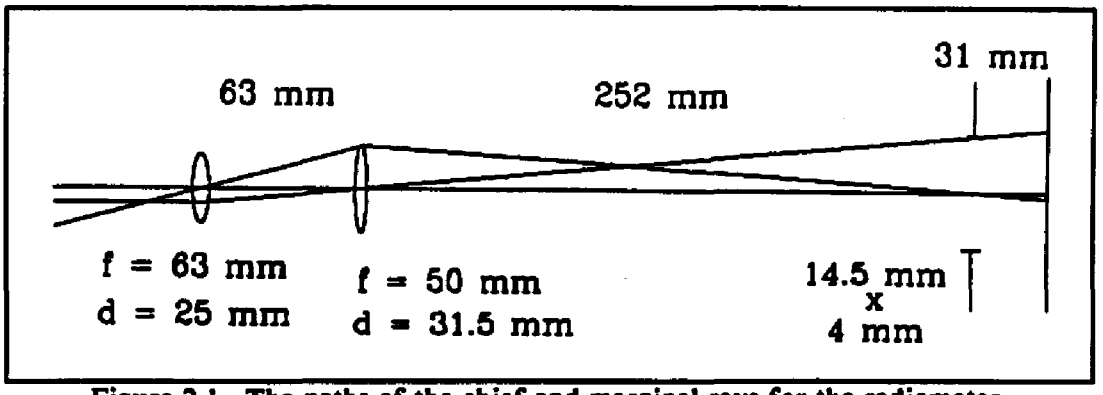

Figure 2.1. The paths of the chief and marginal rays for the radiometer.

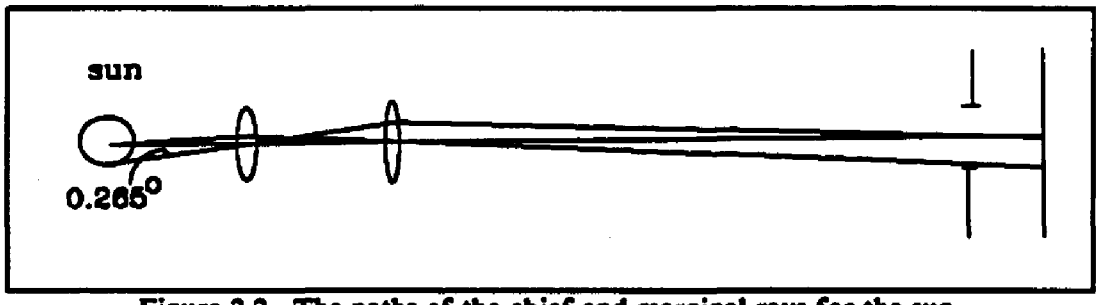

Figure 2.2. The paths of the chief and marginal rays for the sun.

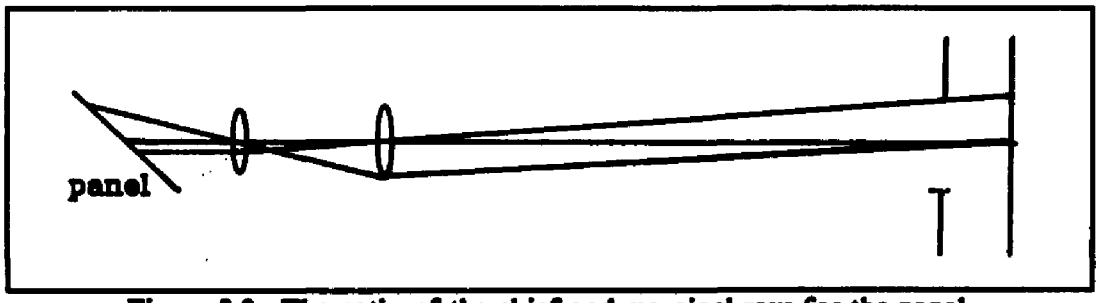

Figure 2.3. The paths of the chief and marginal rays for the panel.

When the radiometer views the panel, its field-of-view (FOV) is completely filled with light. When it views the sun, only a small portion of the FOV receives light, which reduces the ratio of the power detected from the panel and the sun.

Figure 2.2 shows the situation for direct solar irradiation. The image of the sun is formed on or near the field lens, which images the objective lens onto the focal plane. The chief ray is at an

angle of 0.265° to the axis. The image of the sun on the field lens has a size corresponding to the height of the chief ray at the field lens.

Figure 2.3 shows the case for the panel. The assumption that the panel has a diffuse (lambertian) reflectance is made. Its radiance is proportional to its reflectance, the solar irradiance and the angle with respect to the sun. The panel is not in focus, and the radiation accepted is defined by the chief and marginal rays.

RADIOMETRIC ANALYSES

Two different derivations are presented here for describing the radiometry of the ratio measurement. The following variables shown in Figure 2.4 are used in the derivation for the ratio of the RR when viewing the direct sun and a solar-irradiated diffuser panel.

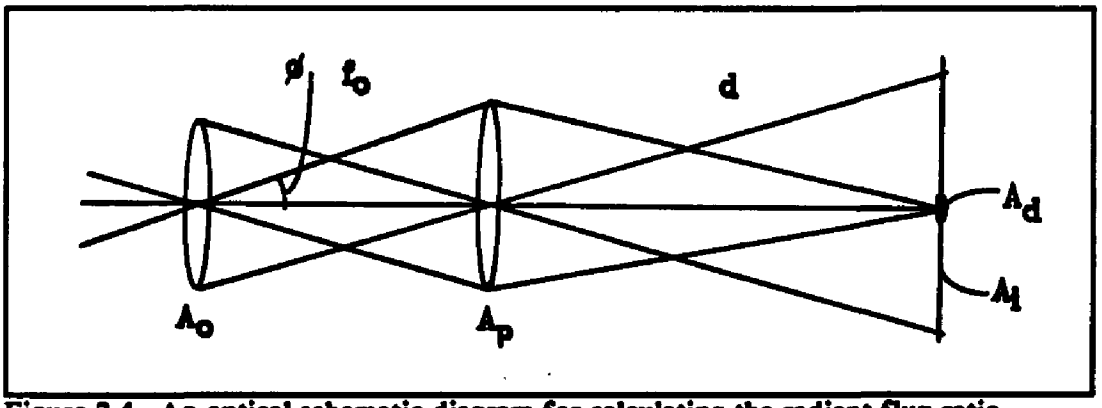

Figure 2.4. An optical schematic diagram for calculating the radiant flux ratio.

A_o = area of objective lens

A_p = area of field stop

A_i = area of objective lens' image

A_d = area of detector

f_o = focal length of objective lens

d = distance between field stop and image plane

m = magnification = d/f_o

Ω = solid angle of radiometer FOV

θ = angle between panel normal and panel-sun line

ϕ = radiometer FOV (half angle)

Φ_s = power on detector from sun

Φ_p = power on detector from panel

τ = transmittance of optical system

ρ = reflectance of panel (assumed lambertian)

E_s = solar irradiance

L_p = panel radiance

(i) First Analysis Method.

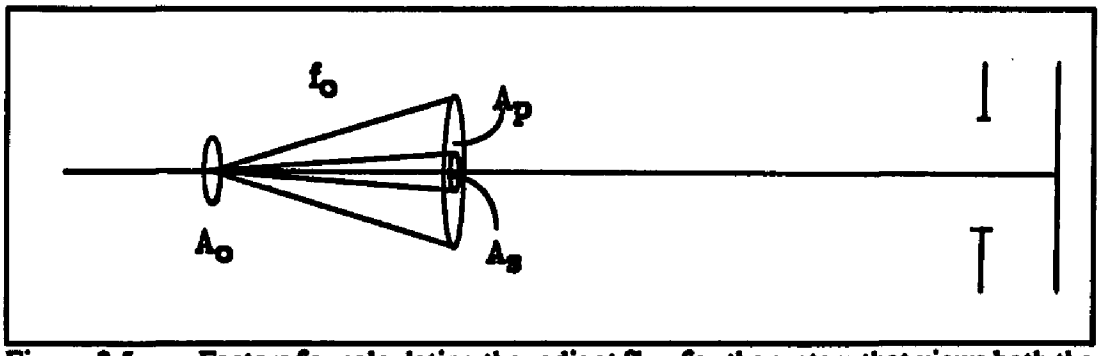

Figure 2.5. Factors for calculating the radiant flux for the system that views both the sun and the panel.

The purpose of the system is to make the ratio of detected radiant fluxes from the sun and panel cases much smaller than the 10^4:1 ratio mentioned previously. The radiant flux in a system is the radiance multiplied by the throughput of the system (product of solid angle and area). Let the radiant flux for the sun and panel be Φ_s and Φ_p respectively. The radiance of the sun, L_s, at 500 nm is $(10^6/\pi)$ W/m^{2}sr(10 nm). The radiance of the panel, L_p, at 500 nm is

$$L_p = \frac{\rho E}{\pi} \cos\theta, \tag{2.1}$$

where ρ is the reflectance of the panel ($\rho = 1$), E is the solar irradiance at the top of the Earth's atmosphere ($E = 20$ W/m^2(10 nm)), and θ is the inclination angle of the panel ($\theta = 45$). Therefore the radiance of the panel, L_p, is equal to $(14/\pi)$ W/m^{2}sr(10 nm). With reference to Figure 2.1 the area of the image of the sun on the field lens, A_s, is 0.2625 mm^2. The total area of the field lens, A_p, is illuminated by the panel and it is 779.3 mm^2. Thus,

$$\Phi_s = L_s A_s \Omega_s = (A_o A_s L_s)/f_o^2 \tag{2.2}$$

and

$$\Phi_p = L_p A_p \Omega_p = (A_o A_p L_p)/f_o^2, \tag{2.3}$$

The ratio of the fluxes is

$$\frac{\Phi_s}{\Phi_p} = \frac{A_s L_s \Omega_s}{A_p L_p \Omega_p} = 24. \tag{2.4}$$

(ii) Second Analysis Method.

The following derivation by Palmer and Slater (1991) gives the ratio in terms of simple panel/radiometer parameters. The only restriction is that the radiometer FOV be large enough to encompass the entire solar disk.

CASE I - Solar irradiation

An image of the sun which is smaller than A_p is formed at the field stop. Therefore, all of the radiant flux ($E_e A_o$) collected by the objective area A_o is transferred to the image plane where it fills A_i. The fraction intercepted by the detector is A_d/A_i. The magnification, m, is d/f_o. Therefore $(A_i/A_o) = m^2$.

$$\Phi_s = E_s A_0 \tau (A_d / A_i)$$
$$A_i = A_0 m^2 \qquad (2.5)$$
$$\Phi_s = A_d E_s \tau / m^2$$

CASE II - Panel irradiation

Radiance is conserved in the system. Therefore, the radiance at the detector is that of the radiance of the panel reduced by the optics transmittance, which is $E_s(\rho/\pi)\tau\cos\theta$. The power on the detector Φ_p is given by $L_p \tau A_d \Omega_d$ where Ω_d is the solid angle of the field stop as seen from the detector, A_p/d^2. The power on the detector is therefore

$$\Phi_p = (E_s(\rho/\pi)\tau\cos\theta) A_p A_d / d^2, \qquad (2.6)$$

and with $d = mf_0$

$$\Phi_p = (E_s(\rho/\pi)\tau\cos\theta) A_p A_d / m^2 f_0^2. \qquad (2.7)$$

The ratio R of the radiant flux from the sun to the radiant flux from the panel is given by

$$R = \frac{\Phi_s}{\Phi_p} = \frac{\pi f_0^2}{\rho A_p \cos\theta} \qquad (2.8)$$

Substituting $\Omega = A_p/f_0^2$,

$$R = \frac{\pi}{\rho \Omega \cos\theta} \qquad (2.9)$$

Therefore, if a ratio of 25 is desired with a reflectance of 0.95 and tilt angle of 45°, the solid angle, Ω, must be 0.187 sr and the FOV (half angle), given by $\Omega = \pi \sin^2\phi$, is 14.1°.

Based on the first analysis, no matter to what extent the transmittance of the radiometer changes, this ratio will remain constant if L_s/L_p remains constant. The only change in L_s/L_p, apart from variation in earth-sun distance, will be due to the changes in the panel radiance. However, this

assumes that the radiometer provides an output which is nearly constant when it is pointed at the sun, i.e., not affected by stray-light changes dependent on pointing accuracy. It also assumes the FOV of the radiometer is less than that subtended by the solar panel at the radiometer so that there are no changes in output signal with small changes in pointing accuracy at the panel.

A ratio near 25 is highly desirable because simple means are available for the accurate determination of a detector's linearity at this ratio. The method, first described by Budde (1982) uses the reflection from a single-surface of SiO_2, calculable from the known index of refraction. For example, if the index is 1.46, the Fresnel equations give a single surface reflectance at normal incidence of 0.033, for a ratio of 28.57. Similarly, borosilicate glass (BK7), with an index of 1.517, has a reflectance of 0.0422 for a ratio of 23.7. The variation, with wavelength and angle, can be easily calculated from known index and dispersion data.

SECTION 2.2: CONSTRUCTION AND CHARACTERIZATION OF A MODEL RADIOMETER

A simple model radiometer was constructed from available lenses, a silicon solar cell detector, and cardboard pieces and tubing. Stray light was reduced with black paint and black flocked paper. A slit aperture was also built from card stock to simulate the aperture of a spectrometer. Each element was mounted in a smaller diameter tube which fit snugly into the outer tube, allowing easy positioning of the elements.

After the model was adjusted to the design specification (Figure 2.1), several measurements were taken to demonstrate its characteristics. To measure the FOV of the radiometer, scans were conducted using the sun as source with the RR mounted on a sky scanning instrument with an angular stepping resolution of 0.5 degrees. The influence of the solar aureole noticeably smoothed the profile of the field-of-view. For this reason the following laboratory measurements were made which more closely simulate the geometry of the sun as seen from space.

The radiometer was placed on a motorized turntable with the objective lens centered over the axis of rotation. The detector output was measured using a transimpedance amplifier and a data-logging system which also controlled the rotation of the turntable. The source was a 1000-watt tungsten halogen lamp of type DXW operated from a current-regulated power supply. Data from this test set agreed with the solar measurements mentioned above when the sun was near the center of the field of view. Figure 2.6 shows the response as a function of incidence angle on a linear plot. Notice the reasonably flat top (±2% over ±12°) indicating uniform response over the nominal FOV. Figure 2.6 has a deviation at 8° caused by a chip in the field lens. This uniform response indicates that the pointing for the solar view is not critical. The edges of the FOV also appear quite sharp, which simplifies FOV characterization for the panel view. Figure 2.7 shows the same data plotted in logarithmic form versus angle. This plot demonstrates the excellent out-of-field rejection of this simple model. The performance is considered quite good, especially since no special baffling or other measures were taken to reduce stray light other than the black flock paper and paint. The flight instrument would be designed for even better performance to minimize response from reflections and glints outside the specified FOV.

The data shown in Figure 2.6 were reduced by using a peak-normalization scheme to determine the FOV and solid angle. The values for response for each side of the optical centerline were averaged and it was assumed that the response was axially symmetric. Then a cylinder of equivalent volume was determined, its radius corresponded to a cut-off angle of 12.2°. This angle corresponds to a solid angle, Ω, of 0.14 sr. The ratio for this design, assuming a panel angle of 45° and a panel reflectance of 0.95, is 33.3. This differs slightly from the design from Figure 2.1, which has a field half-angle of 14.5° and a ratio of 24.

Measurements were taken in natural sunlight to verify the ratio using the radiometer. It was first mounted on a tracking platform to determine the signal for direct solar input. It

was then pointed at a $BaSO_4$ panel (reflectance = 0.95) placed at an angle of 45° with respect to the sun. The measured ratio was 26. This number differs from the predicted ratio of 33.3 because the increased panel radiance due to diffuse sky radiation was not take into account.

Figure 2.7. FOV OF RATIOING RADIOMETER

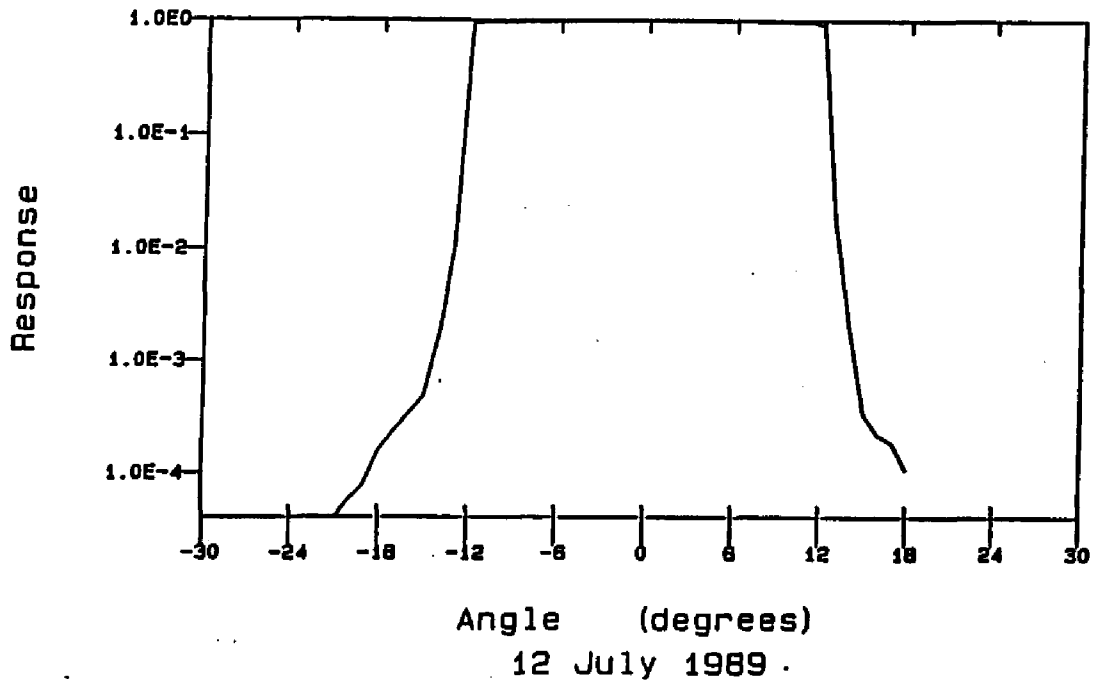

Figure 2.6. FOV OF RATIOING RADIOMETER

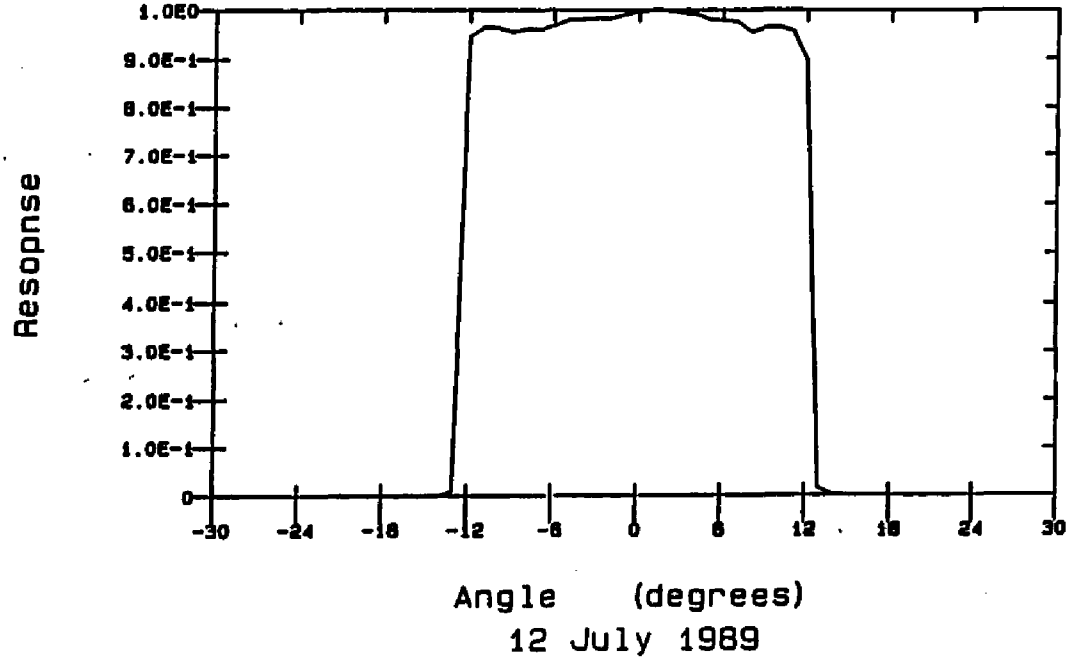

SECTION 2.3: ERROR ANALYSIS

This section details the analysis of some of the known possible sources of error in the RR. Two cases are presented: the first occurs when no stray radiation sources are present and the second includes the effects of stray radiation. The emphasis now shifts from an analysis of the ratio, which was useful for the initial design of the RR, to an analysis of the panel radiance, L_p, the desired quantity for the in-flight calibration of the multispectral satellite sensor. The overall goal is to measure the panel radiance, L_p, with a maximum R.S.S. uncertainty of 1.5% with respect to the solar constant over a 10-year period.

There are a number of assumptions to begin with. First, it is assumed that the sun irradiance, E_s, is stable. (Its actual value can be used when needed by reference to the latest, most reliable determinations.) The entire in-flight calibration process rests upon this assumption. It is known from long-term monitoring of the total solar output that the variation is less than 0.2% (Willson and Hudson, 1988). The most variable portion of the solar spectrum is in the ultra-violet. This sets an upper bound on variations in the visible and near-IR, which can be no greater than 0.2% (Lean, 1989).

Second, it must be assumed that the calibration panel overfills the field of view of both the multispectral satellite sensor and the RR. If the panel does not fill the FOV, either due to panel sizing or erroneous pointing of the multispectral satellite sensor, then an unknown background will be in a portion of the field viewed and the panel area must be accurately known. Third, the assumption made is that materials chosen for the RR do not exhibit solar-induced luminescence, which would add or subtract to the signal in some wavelength regions and would behave differently for solar and panel illumination. Fourth, it is assumed that there is no extraneous source of radiant flux present due to a glowing of the very thin

atmosphere surrounding the space platform (in another context called "Shuttle glow") (Chen 1987 and Hunton 1989).

Several of the anticipated error terms are readily predictable, while others can only be estimated. The task is to assign values to the known error sources and then ensure that the goal can be met with realistic uncertainties for the remaining sources. Palmer (1991) discusses two cases: (1) No stray radiation, where the only source is the direct sun incident on the radiometer and the panel respectively; and, (2) where other portions of the spacecraft act as secondary sources for both the RR and the panel. Some errors are common to both cases, and others are exclusively related to stray radiation.

A potential source of error is the result of the difficulty in assessing the effect of solar-induced luminescence from the solar ultra-violet excitation of certain materials, both organic and inorganic, causing them to emit light at longer wavelengths. The luminescent emission is mainly in the visible portion of the spectrum. It should be ensured that the materials chosen for the optics, the panel, and all surfaces within the RR FOV are free from luminescence. The troublesome issue is luminescence from contaminants deposited on the surfaces of the panel and on the RR entrance optics. These surfaces should be stowed most of the time to minimize the deposition of contaminants. If the entrance optics of the RR are covered with a luminescent material, then the RR output will be higher for the direct solar view than for the panel view, increasing the ratio R, which lowers the apparent value of L_p. If, on the other hand, the panel becomes contaminated, its radiance might increase, lowering the ratio R and increasing the apparent value of L_p. Over the duration of the mission, this effect may cause variations in the ratio R from negligible in certain spectral regions (1000-2500 nm) to a high percentage in portions of the visible spectrum. Of utmost importance are the identification of luminescent materials that can deposit onto components, and, determination of their abundance with respect

to time. For now, an uncertainty of 1% is assigned to the value of the ratio because of this problem.

The panel must be flat (to preclude the possibility of a radiance gradient across the panel) and must stay flat throughout repeated thermal cycles. The mechanical mounting should feature hard stops so that the panel position is repeatable.

The panel and the RR FOV have been computer-modeled to understand the uncertainty due to an uneven panel radiance. From Figure 2.6, the FOV response decreases as it moves away from the FOV center. For modeling purposes, the FOV has a value of unity at the center, decreasing linearly to 0.95 before falling to zero. The panel has a value of unity and changes linearly by ±0.02 at the ends, see Figure 2.8. The RR response is found by moving the FOV across the panel where the FOV is completely within the panel limits. The response is a straight line which only varies ±0.4%, Figure 2.9.

Figure 2.8. RATIOING RADIOMETER

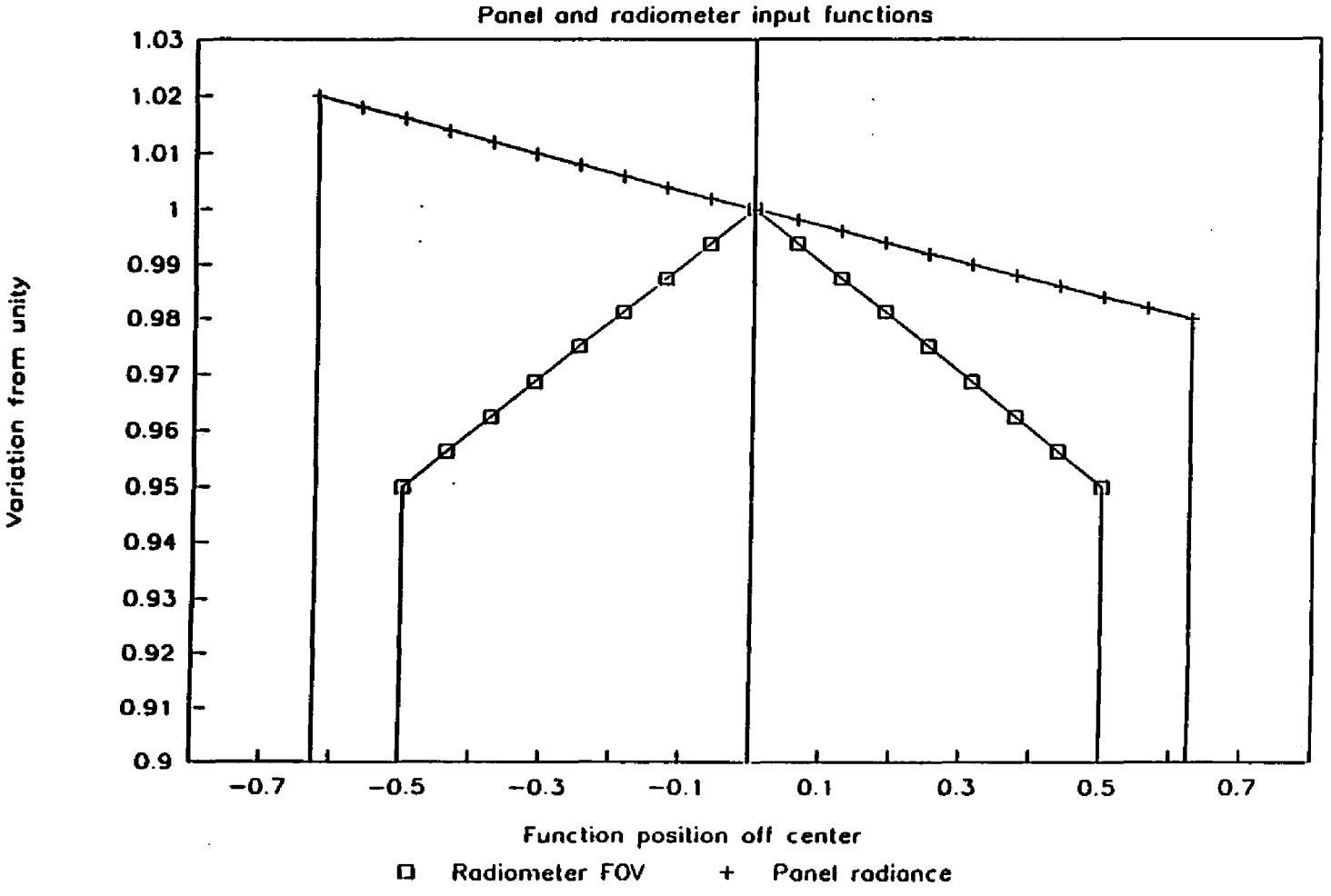

Figure 2.9. RATIOING RADIOMETER

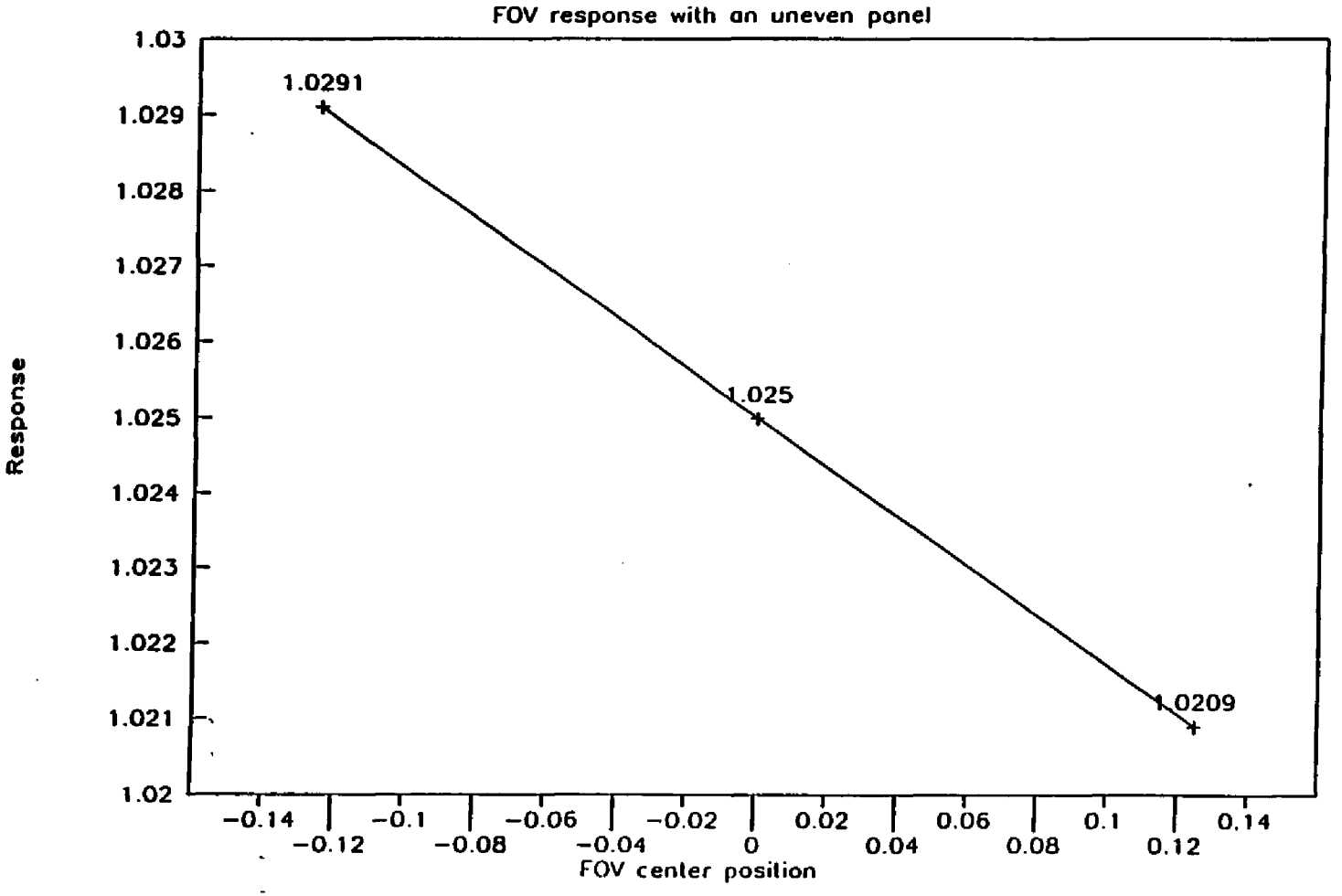

Table 2.1 summarizes Palmer's (1991) calculations, estimates and educated guesses and shows the R.S.S. (root-sum-square) estimates of the total uncertainty. Since the effects of solar-induced luminescence are unknown at this time, the totals are given with and without the estimates of the effects of this error source. Cases I and II are for no stray radiation and for stray radiation on the panel. The results show that the error in the calibration system can be less than two percent depending on whether or not there is luminescence present.

Finally, the conclusions that can be drawn from observations of the RR over time are noted. It is assumed that both outputs, one for the direct solar view and the other for the panel view, are available in the data stream. It is also assumed as before that E_s is stationary. If a drift in the readings when observing the sun is seen, then a drift in the characteristics of the RR is inferred. On the other hand, a change in the ratio, R, implies that a change in the radiance of the diffuser has occurred.

Table 2.1. Summary of Estimated Percentage Errors.

ERROR SOURCE	CASE I	CASE II
RR SOLID ANGLE (calc)	0.5	0.5
FOV UNIFORMITY (calc)	0.5	0.5
PANEL BRDF (est)	0.5	0.5
RR LINEARITY (est)	0.25	0.25
DATA TIMING (calc)	0.5	0.5
LUMINESCENCE (guess)	1.0	1.0
PANEL POSITIONING & FLATNESS (est)	0.25	0.25
PANEL SPATIAL UNIFORMITY (calc)	0.4	0.4
STRAY LIGHT, SPACECRAFT REFLECTIONS (guess)	0.0	1.0
STRAY LIGHT, EARTHSHINE (guess)	0.0	1.0
TOTAL R.S.S. ERROR (no luminescence)	1.13	1.81
TOTAL R.S.S. ERROR (with luminescence)	1.51	2.07

CHAPTER III

DIFFUSER PANEL MATERIAL SELECTION

This chapter discusses the selection of a diffuser panel material for long duration use in the space environment. Section 3.1 lists the desirable characteristics that the diffuser panel should retain. Section 3.2 discusses the selection of the different materials. Section 3.3 describes the tests performed on the sample materials including the proton exposure and ultraviolet radiation tests. Section 3.4 analyzes the results.

A luminescence test, initial spectral bidirectional reflectance factor (BRF) and directional-hemispherical spectral reflectance measurements were performed at the University of Arizona. The spectral BRF scan determined the specular and diffuse angular reflectance distributions of the materials at several wavelengths, 425, 500, 750, 1650, and 2220 nm. The directional-hemispherical spectral reflectance properties were measured by a spectrophotometer generally over the range from 400-2000 nm. One of each type of sample was then sent to California Institute of Technology for proton exposure. The samples were returned to the University for the spectral reflectance measurements to be repeated and for polarization and depolarization measurements to be made at 500, 750 and 950 nm. Selected samples were sent to TRW for ultraviolet irradiation. These samples were also returned to the University for the same measurements.

Only the optical degradation of the diffuser panel material in the space environment (solar radiation, local spacecraft contamination, and particles in space, such as protons and atomic oxygen)

is discussed in this chapter. Before deciding on a material, both the thermal and mechanical properties (e.g., hardness, thermal expansion, mountability) must also be taken into consideration.

SECTION 3.1: DESIRABLE DIFFUSER PANEL MATERIALS

Suggested preliminary optical specifications for the panel are that: 1) The spectral reflectance should have a minimum value of 0.6 and preferably an average value above 0.8 across the entire spectral range of interest; 2) The spectral reflectance should be slowly-varying or uniform to minimize the number of spectral bands needed to monitor the panel; 3) The directional reflectance should remain within ±0.5% for a change in viewing angle of ±10° under the same illumination conditions with no more than a 20% specular component; 4) The spectral and spatial characteristics should not degrade more than 2% for the duration of the mission (5 years); 5) The uniformity of reflectance over any 1-cm^2 area should be ±0.5% of the average panel value; and 6) The material should not exhibit measurable luminescence when irradiated by exoatmospheric solar flux, because of the uncertainty this would introduce in predicting its radiance.

The panel should not be easily contaminated which implies low "stiction" to repel particulates, low adsorption and absorption for gaseous materials and as close to neutrally charged as possible to avoid attraction of ionized particles. Good rejection helps to eliminate the change in reflectance of the panel caused by particle contamination. It also reduces the possibility of increased panel radiance due to particle luminesce.

SECTION 3.2: DIFFUSER PANEL MATERIAL CANDIDATES

This section details the initial selection of materials and specifies which materials were selected for proton exposure and intense ultraviolet irradiation.

Table 3.1 lists the samples tested, their characteristics and the suppliers of the samples. Of these 12 samples only two were initially eliminated because they did not meet the panel characteristics mentioned in Section 2. Sintered silicon nitride (Si_3N_4) has a dark gray color, which was considered undesirable for the panel. The fused silica (SiO_2) sample was excluded because it was chalky and would probably not hold up very well in the space environment.

Table 3.1. Diffuser panel candidate materials.

Sample	Sample Size and Quantity	Thermal Stability	Color	Luminescence	Supplier	Comments
Spectralon*	four - 2.5-cm optical-grade & six - 3.8-cm laser-grade	Stable to 325°C; heat expansion	White	Purple	Labsphere, N. Sutton, NH	Near lambertian; 25.4 or 45.7-cm square or mosaic
Sintered Halon	two - 4.8-cm	Heat expansion?	White	Purple	Jack Hsia NIST	Near lambertian
Macor#	two - 2.5-cm	1000°C max.	White	No	Corning Dr. J. M. Palmer	
Pyroceram#	one - 7.6-cm square	700°C cont.; 800°C intermit.	White	No	F. J. Gray Jamaica, NY	Not currently being made
SiO_2 Fused silica	two - 2.5-cm		White	Untested	GTE Wesgo Belmont, CA	
Al_2O_3 Alumina 99.9%	four - 2.5-cm	1900°C max.	White	No	GTE Wesgo Belmont, CA	
Si_3N_4 Sintered silicon nitride	three - 2-cm	1200°C max.	Gray	Untested	GTE Wesgo Belmont, CA	
Porcelain enamel on steel	one - 21-cm & two - 3.2-cm		White	No	Erie Ceramic Arts Co.	
IITRI S13G/LO-41‡	two - 2.5-cm		White	No	IITRI Chicago, IL	Good atomic oxygen rejection
IITRI YB-71‡	two - 2.5-cm		White	No	IITRI Chicago, IL	Good atomic oxygen rejection
IITRI Z-93†‡	two - 2.5-cm	650°C no adverse effects	White	Yellow	IITRI Chicago, IL	Good atomic oxygen rejection

* Labsphere, Inc, 1990.
# Corning Glass Works, 1980.
‡ Harada, 1990
† Harada, 1983

Three of the candidate materials are polytetrafluoroethylene (PTFE) compounds: optical- and laser-grade Spectralon from Labsphere and sintered Halon from NIST. The optical-grade Spectralon has a higher reflectance than the laser-grade, while the laser-grade Spectralon has less specularity, Springsteen (1991). The laser-grade Spectralon has a less contaminated resin PTFE powder base than the optical-grade Spectralon.

Luminescence was tested by placing a strong ultraviolet (UV) source (Philips 90-watt 93110E Hg-in-Qtz) in a black room (i.e., reflectance less than 0.05 for most wavelengths) behind a filter which transmitted around 254 nm (>40%) and absorbed visible wavelengths longer than 400 nm (<10% transmittance). Another filter that absorbed wavelengths below 380 nm was used to check that luminescence did not occur when the UV from the lamp was blocked. The samples were placed about 20-cm from the filter. Inspection of the candidate materials was made visually, see Figure 3.1.

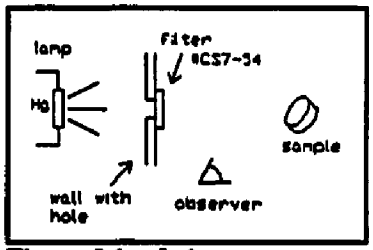

Figure 3.1. Laboratory set-up for the luminescence test.

Known luminescent and non-luminescent materials were tested to check the setup and help the observers understand what to expect. Materials which luminesced would "light-up" when UV radiation was present and would become nearly invisible when it was not. The non-luminescent materials were nearly invisible with and without UV irradiation.

The materials which luminesced included all the PTFE compounds (Spectralon and sintered Halon) and the IITRI paint Z-93. Also, additional samples of Halon powder and pressed Halon were tested to see if the luminescence was inherent in the PTFE compounds. All the PTFE compounds luminesced with a strong purple color only when UV light was present. The Z-93 paint had a strong yellow emission when UV light was present.

In spite of their luminescence, all these materials underwent proton exposure and UV-irradiation. The Z-93 paint has proven itself in the space environment for low outgassing and small

degradation over time. The PTFE compounds are fairly new, have never been tested for space use, and considered prime candidates due to their near-lambertain behavior.

SECTION 3.3: TEST PROCEDURE

This section outlines the procedure and facilities used in testing the sample materials for proton- and ultraviolet-induced degradation and for their polarizing and depolarizing properties.

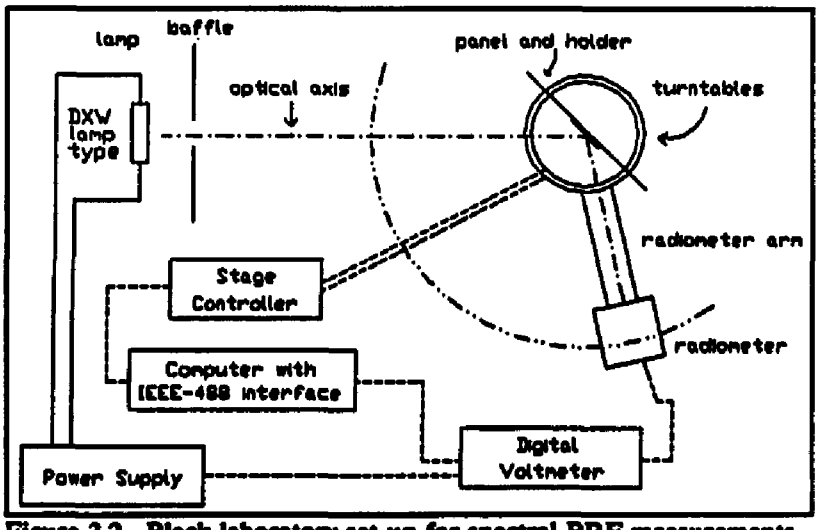

Figure 3.2. Black laboratory set-up for spectral BRF measurements.

The spectral BRF measurements were made using a lamp (1000-watt tungsten halogen lamp, type DXW) housed in a black box with a circular aperture along the optical axis (see Figure 3.2). The lamp current was controlled with a constant-current regulated power supply. The panel materials were placed sequentially at the center of rotation of one of two coaxial turntables with an incidence angle of 45°. A radiometer was attached to an arm on the second turntable which provided a scan of the panel from 0° to 60° in 5° increments.

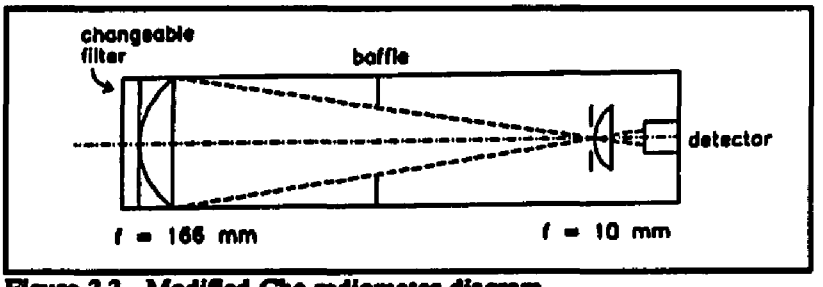

Figure 3.3. Modified Che radiometer diagram.

Two radiometers were used to obtain the wavelengths needed. For the wavelengths 425, 500 and 750 nm, a modified Che radiometer with a 1° FOV (built at the University of Arizona by Che Nianzeng) was used (see Figure 3.3). The radiometer was modified, by changing the objective lens to a longer focal length, so that the sample filled its FOV when the angle of the radiometer to the surface normal was less than 60°.

A Barnes Modular Multispectral 8-Channel Radiometer (MMR), Barnes Engineering Co., was used at center wavelengths of 1650 and 2220 nm. The MMR is a portable, battery-operated instrument containing eight simple, independent, optically-chopped radiometers. Four channels are in the visible and near infrared (VNIR) spectrum, three are in the short-wave infrared (SWIR), and one channel is in the thermal infrared (TIR) spectrum. The radiometer has an ill-defined nominal 1.0° FOV in the SWIR that extends beyond 10° according to Che et al (1984). An exterior baffle was built to limit the spread to a well-defined 3.0° FOV. Because the MMR FOV covered an area approximately 5-cm in diameter at normal incidence to the samples, the samples were surrounded by a black material (less than 1% reflectance in the IR) and a cosine fall-off correction was used to determine their reflectance. The two channels used have filtered wavelength regions of 1550 to 1750 and 2080 to 2350 nm with peak transmittances at 1650 and 2220 nm. Each individual radiometer consists of: a filter, lens, detector (see Figure 3.4), and a temperature compensating thermistor, and gain-adjustable preamplifier. A four-blade chopper, driven at 50 Hz by a brushless DC motor with accurate speed control electronics, provides optical chopping for all channels.

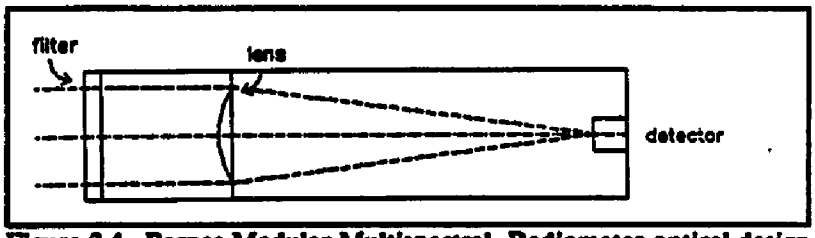

Figure 3.4. Barnes Modular Multispectral Radiometer optical design for 1° FOV. (The lens is removed to provide a 15° FOV.)

The directional-hemispherical reflectance measurements were performed on a Cary 2415 spectrophotometer with an integrating sphere attachment (Varian, 1990). It makes use of a scanning monochromator to cover the wavelength region which, in general, was from 400 to 2000 nm. The upper and lower limits varied depending on the sample reflectance. The Cary 2415 determines the ratio of the directional-hemispherical reflectance of a sample to a known reference reflectance (Spectralon).

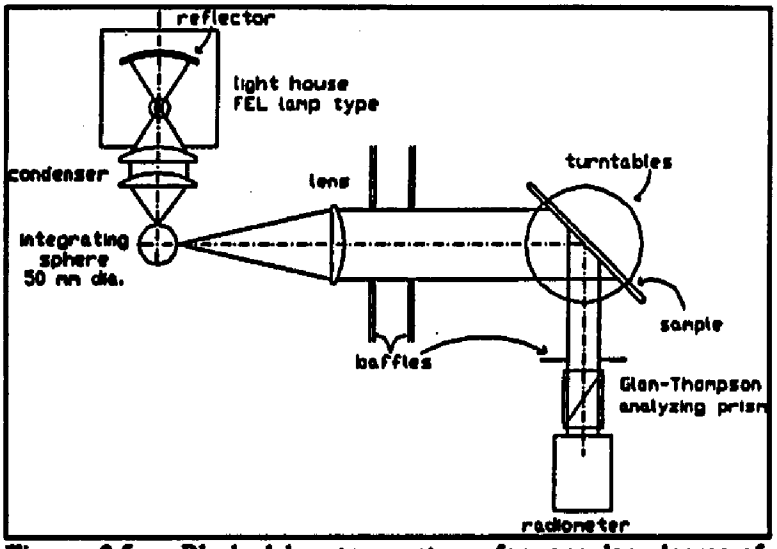

Figure 3.5. Black laboratory set-up for angular degree-of-polarization measurements.

The angular polarization measurements were made using the arrangement in Figure 3.5. Light from a 1000-watt quartz-line lamp, type FEL, was directed through a condenser into a 50-mm diameter integrating sphere. The sphere transmitted light with less than 2% polarization into a collimating system which illuminated the sample on one turntable. A Glan-Thompson polarizer, having an extinction

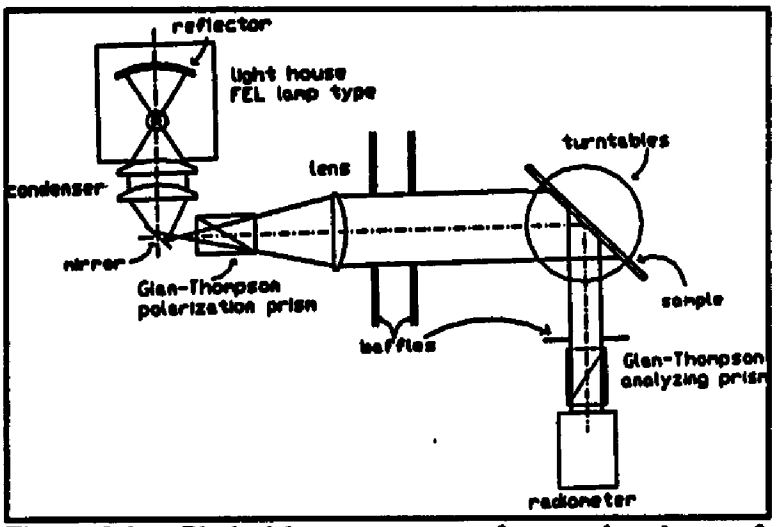

Figure 3.6. Black laboratory set-up for angular degree-of-depolarization measurements

ratio of 10^{-5}, was placed in front of the radiometer on the arm attached to the other turntable that is coaxial with the first. Angular scans were then made for vertical and horizontal directions of polarization. To determine the depolarization of the samples, the integrating sphere was replaced by a mirror at 45°, and a Glan-Thompson polarizing prism set at 180° was placed between the mirror and collimating lens, Figure 3.6. Two baffles were used to prevent the beam from expanding and these kept the edge of the beam as well defined as possible. The sample was illuminated with this light at a 45° angle. A Glan-Thompson analyzer was placed between the sample and the detector. A small baffle was placed in front of the analyzer to exclude stray-light. The output of the detector was monitored as the analyzer was rotated from 180° to 90°. The polarization was measured for different angles of the radiometer with respect to the sample and with the different filters previously mentioned. The degree of polarization, P, and the degree of depolarization, D, are defined as

$$D = P = \frac{\rho_{90^\circ} - \rho_{180^\circ}}{\rho_{90^\circ} + \rho_{180^\circ}} \tag{3.1}$$

where ρ is the reflectance of the sample. By degree of depolarization we mean the residual polarization after scattering off the diffuser material.

Proton exposures were conducted at the proton-accelerator facilities at California Institute of Technology. A 10-cm-diameter proton beam was used to irradiate the samples with 10^{10} p/cm^2 at energy levels of 1 keV, 1 MeV, and 10 MeV, Bruegge, et al, 1990. These values are representative of fluence levels accumulated during a five-year Eos mission. The pressure in the chamber was below 5×10^{-5} torr throughout the experiment. The particle count was controlled by a switch that shut off the beam current after a Faraday cup, mounted in the target chamber in the center of the proton beam, measured the desired count. Four samples were irradiated each run. Two witness samples, placed in the chamber outside the particle beam, helped to characterize the contamination in the chamber during the test. A diffuse sample of Spectralon and a specular sample of solar-reflector material were

used as witness samples. The samples were held in place by aluminum rings, fastened with screws and bolts.

The ultraviolet (UV) irradiation tests used facilities at TRW, Gilmore, 1990. Each sample was placed in a small vacuum chamber. The sample was clamped at the end of a water-cooled shaft and enclosed in a fused-silica tube. The chamber unit was first evacuated using a carbon vane and "Vacsorb" pumping station. Once the vacuum unit was sufficiently evacuated, it was sealed using all-metal valves and then maintained at vacuum using an 8 liter/sec ion pump. The pressure in the sample container was monitored by measuring the pump ionization current. A 5 kilowatt short-arc Xenon lamp was used as an ultraviolet source for exposure of the sample. The sample, while in vacuum, was placed at the appropriate distance from the lamp for the desired irradiation (Figure 3.7). The samples were irradiated with 1.5 equivalent suns for 333 hours, yielding 500 equivalent hours exposure. For a five-year mission with ten minutes per calibration, this is equivalent to 11 calibrations per week.

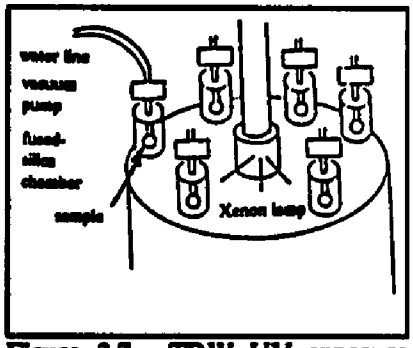

Figure 3.7. TRW UV exposure facility.

SECTION 3.4: TEST RESULTS

This section is divided into four parts: 1) results of the pretest Cary 2415 spectrophotometer and bidirectional reflectance factor measurements; 2) comparison of the measurements in 1 above to measurements after proton exposure; 3) the polarization measurement results for the proton-exposed samples; and 4) comparison of the pretest results and proton results to the results of the samples after UV irradiation. To condense the description of the results, the candidate materials were separated into three classes: ceramics (Al_2O_3, Macor, Porcelain and Pyroceram), PTFE compounds (sintered Halon and Spectralon) and IITRI paints (S13G/LO-41, YB-71 and Z-93).

When examining the BRF data it is important to note that those taken beyond 40° are questionable because the exact replication of the black laboratory conditions after each test was difficult as was the pointing of the two radiometers at precisely (< ±1-mm error) the center of each sample. However, during pretesting, Al_2O_3 samples were measured at two different times with the Che radiometer and the reflectance data were within 3% of each other. The error in the placement of each sample, from exactly 45° to the light source for the BRF measurements, is evident from the position of the specular component which varies from 45° by an average of ±2°. This error is due to the limited sample size and mounting arrangement, not the turntable accuracy.

The polarization data were taken on the proton-exposed and UV-irradiated samples and not on the pretest samples because the polarization equipment was not set up in time. The small degrees of polarization and depolarization measured after proton exposure are of little concern and it is unlikely that the unexposed surfaces showed any significant difference.

PRETEST RESULTS

CARY MEASUREMENTS

The initial Cary 2415 diffuse reflectance measurements (Figures 3.8a through 3.17b) showed that all the candidate materials meet the specular reflectance requirements for the wavelength range of 0.4 to 2.0 μm provided they do not change in the space environment. The samples were referenced to the same Spectralon sample throughout the testing procedure. (The spikes at about 0.55 μm, seen on several graphs, were caused by the Cary changing detectors not by any characteristic of the sample.)

Al_2O_3 had a reflectance near 100% decreasing to 65% at 0.4 μm. The other three materials, Macor, Porcelain and Pyroceram, had distinctive high and low reflectance points, but the fluctuations were gradual and distinctive. Pyroceram had the lowest of reflectance values, with a minimum of 6% and a maximum of 76%. Porcelain decreased linearly with wavelength above 0.5 μm.

The sintered Halon and Spectralon samples had reflectance values approaching 100% with little variability.

The three IITRI paints all had roughly the same spectral reflectance values. Between 0.5 and 1.4 μm, the average reflectance value was about 97%. S13G/LO-41 had two distinctive downward spikes at about 1.6 μm and 1.65 μm. Unlike the other paints, YB-71 did not decrease rapidly in reflectance value below 0.5 μm.

BRF MEASUREMENTS

As depicted in Figures 3.18, 3.24 and 3.26, most ceramics, except Macor (Figure 3.21), contain a specular component. Al_2O_3 had the smallest specular component, Porcelain was next and Pyroceram had the largest. Al_2O_3 was the only ceramic sample that had a BRF above 0.75 for all wavelengths. Pyroceram had the lowest reflectance; 0.71 at 500 and 750 nm, 0.63 at 425 nm, 0.163 at 1650 nm and 0.063 at 2220 nm.

The BRF in the VNIR is approximately 1.0 for all the PTFE compounds (Figures 3.29, 3.32 and 3.35). The SWIR reflectances were 10% lower than the VNIR reflectances. The two Spectralon samples had roughly the same reflectance values at 1650 nm.

All the IITRI paints had approximately the same BRF (Figures 3.37, 3.39 and 3.42) with reflectance between 0.9 and 1.0 in the VNIR and a reflectance of 0.7 to 0.8 in the SWIR. Above 30 degrees, the BRF at 2220 nm showed the most variance between samples.

RESULTS AFTER PROTON EXPOSURE

No visible change in the appearance of the samples was observed after proton exposure.

CARY RESULTS

Proton exposure on the ceramics, Figures 3.8a through 3.11, had the effect of either appearing to clean the surface and thereby increase the diffuse reflectance or to have no effect. Pyroceram

(Figure 3.11) showed the only significant change in reflectance with an unexplained increase from 0.11 to 0.44 at 2 μm.

All the PTFE compounds, Figures 3.12 through 3.14, exhibited a slight decrease in the diffuse reflectance.

An overall decrease in reflectance occurred in both S13G/LO-41 and YB-71, whereas an overall increase in reflectance occurred with Z-93.

BRF RESULTS

The different ceramics exhibited very different BRF response after proton exposure. Al_2O_3, Figure 3.19, decreased at 425 and 500 nm, and increased at 1650 and 2220 nm. The specular component for Al_2O_3 increased. The BRF for Macor, Figure 3.22, increased in the SWIR. Porcelain, Figure 3.25, stayed virtually the same except that no specular component can be seen at 2220 nm, whereas in the pretest results showed a strong specular component. At 1650 nm the specular component increased greatly. The spectral BRFs in the VNIR varied considerably, at 425 nm the increase was greatest while at 750 nm the increase was small. The SWIR specular component for Pyroceram increased with wavelength. In the VNIR the values were uncertain because the detector saturated.

The PTFE compounds all had approximately the same BRF in the VNIR. In the SWIR the BRF for the laser-grade Spectralon changed the least. The maximum change occurred at 1650 nm with an increase in the optical-grade Spectralon, Figure 3.33.

The IITRI paints all exhibited a slight decrease in BRF in the VNIR. At 1650 nm there was an increase for all the IITRI paints. At 2220 nm YB-71, Figure 3.40 and S13G/LO-41 increased.

POLARIZATION MEASUREMENTS

The degree of polarization follows a similar pattern for all the samples, it was generally less than 3% and decreased as the angle of illumination increased. Of all the samples, Macor changed the

most at 950 nm from 0.025 at a 10° angle of illumination to -0.007 at 65°. At 500 nm Pyroceram exhibited a different behavior, it increased in degree of depolarization from -0.08 at 10° to 0.015 at 25° then decreased to 0.007 at 65°. The -0.08 value at 10° for Pyroceram is thought to be due to the reflection being near specular.

The degree of depolarization decreased with increasing angle of illumination for ceramics, Figures 3.46, 3.48, 3.50 and 3.52. Pyroceram, Figure 3.52 had the greatest degree of depolarization with 0.14 at 950 nm and 0.122 at 500 nm for a 10° angle of illumination, it decreased to 0.077 and 0.08 respectively at 65°. Porcelain changed the least with the angle of illumination and Macor had the smallest degree of depolarization with 0.031 at 500 and 950 nm and 0.024 at 750 nm.

The optical-grade Spectralon, Figure 3.56 had about twice the degree of depolarization of the other two PTFE compounds, Figures 3.54 and 3.58 with 0.012 at a 10° angle of illumination. In general, as the angle of illumination increased, the degree of depolarization decreased to -0.029 ± 0.004 at 65°. The exception was sintered Halon which decreased to -0.017.

The degree of depolarization for the IITRI paints follows the same pattern, decreasing as the illumination angle increased, but each behaved differently as a function of wavelength. S13G/LO-41 had the only two curves which cross each other, for the wavelengths of 500 and 950 nm. YB-71 and Z-93 exhibited about a 0.008 separation between wavelengths. YB-71 had the greatest degree of depolarization of the three paints with 0.035 to 750 nm decreasing to 0.004 at a 65° angle of illumination. Z-93 had the lowest degree of depolarization with 0.012 at 950 nm decreasing to -0.028 at a 65° angle of illumination.

RESULTS POST UV IRRADIATION

The samples that were UV irradiated were Al_2O_3, Macor, Pyroceram, sintered Halon, optical-grade Spectralon, S13G/LO-41, YB-71 and Z-93. After the UV irradiation, all of the samples except

Pyroceram appeared brown. The sintered Halon and Spectralon were the darkest brown and the IITRI paints visually appeared to be the least affected. Pyroceram had a light blue-gray tint.

CARY RESULTS

All the ceramics, Figures 3.8b, 3.9 and 3.11 decreased in diffuse reflectance below 0.7 μm.

Both PTFE compounds decreased in diffuse reflectance from pretest and proton exposure below 1.0 μm with a steady decrease to 0.2 μm. The maximum decrease was 65% for optical-grade Spectralon and 40% for sintered Halon, Figures 3.12 and 3.13. Otherwise, the diffuse reflectance of the PTFE compounds remained close to their pretest and post proton exposure values.

The IITRI paints decreased in diffuse reflectance from pretest between the wavelengths of 0.3 and 0.7 μm. S13G/LO-41, Figure 3.15b, showed a more pronounced structure than before and appeared to be dirty, therefore only its diffuse reflectance was measured. YB-71 decreased 18% at 0.33 μm and Z-93 decreased 14% at 0.4 μm. Z-93 increased around 1.9 μm.

BRF RESULTS

Both Al_2O_3 and Macor, Figure 3.20 and 3.25, exhibited severe decreases in BRF at 425 nm. Al_2O_3 stayed close to the pretest and proton exposure BRF at 500 and 750 nm and increased from pretest reflectance values at 1650 and 2220 nm, while decreasing at 1650 nm increasing at 2220 nm after proton exposure. The specular components for Al_2O_3 increased. Macor stayed about the same, except at 2220 nm where it decreased post proton exposure. The BRF for Pyroceram decreased at 750, 1650 and 2220 nm. Since the specular component for Pyroceram was very large, it could not be seen if the specular component changed.

After the UV irradiation (Figures 3.31 and 3.34), the BRF for all the wavelengths of the PTFE compounds decreased from their pretest and proton exposure BRF values. The maximum decrease for both pretest and post proton exposure was seen at 425 nm with a decrease of 31% for sintered Halon and 41% for optical-grade Spectralon, Figure 3.34.

In general the BRFs of the IITRI paints, YB-71 and Z-93 (Figures 3.41 and 3.44), changed in the same way to UV irradiation, but to a different extent. YB-71 decreased from pretest at 425 and 2220 nm. Z-93 differed the most with a decrease at 425 nm. With respect to the proton exposure, both paints decreased by approximately the same percentage difference. The only exception was at 2220 nm where Z-93 slightly decreased.

POLARIZATION RESULTS

The degree of polarization generally decreased with increase in illumination angle, Figures 3.51 and 3.55. The degree of polarization did not differ widely from the proton exposed samples and did not exceed 3%.

The degree of depolarization increased at 500 nm an average of 0.005 for Macor and 0.01 for Al_2O_3. Pyroceram (Figure 3.52) exhibited an average increase of 0.02 at 750 nm, for a maximum increase, and 0.006 at 500 nm. The degree of depolarization stayed approximately the same for Pyroceram at 950 nm. The increase of Pyroceram at a 10° angle of illumination was probably cause by the proximity of the specular angle.

The degree of depolarization for UV-irradiated sintered Halon (Figure 3.56) was greater than it was for the proton exposed sample. The depolarization decreased with a difference of 0.015 at 10° to near 0.003 at 65°. There was an average difference at 750 nm of 0.025. At 950 nm the degree of depolarization exhibited a 0.006 difference at 10°, no difference around 40°, and a difference of -0.005 at 65°. Optical-grade Spectralon, Figure 3.58 did not differ more than ±0.003 at 750 and 950 nm, but at 500 nm there was an increase in the degree of depolarization with an average difference of 0.013.

The degree of depolarization was within ±0.004 at 500 and 950 nm for both paints. At 750 nm the degree of depolarization for both paints decreased but Z-93 decreased slightly (an average of 0.002), whereas, YB-71 decreased by an average of 0.018.

Figure 3.8a. Al_2O_3 #3
Cary data: Reference to halon

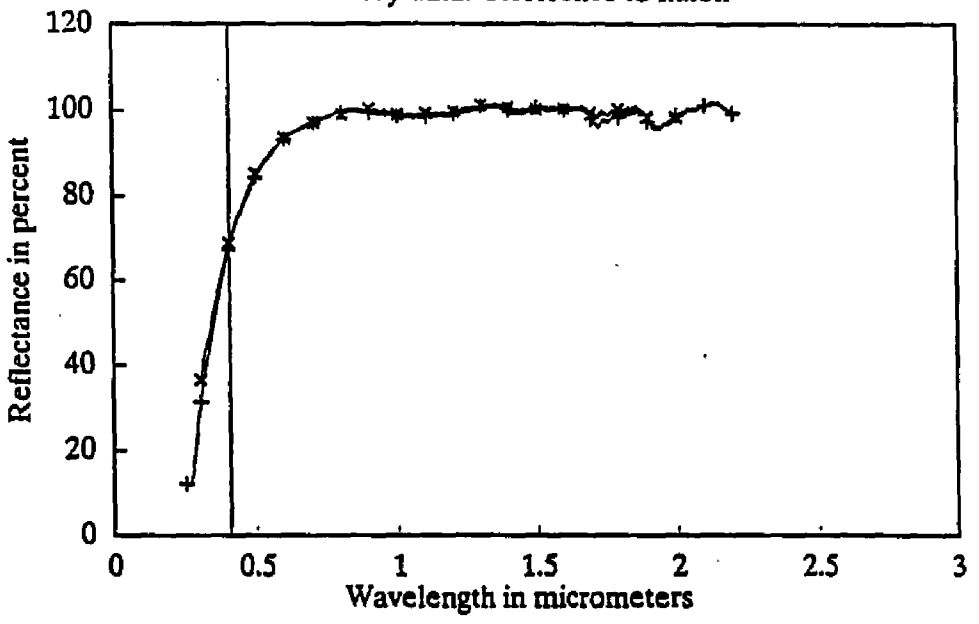

× pretest: 30 July 1990 + proton: 21 August 1990

Figure 3.8b. Al_2O_3 #1
Cary data: Reference to halon

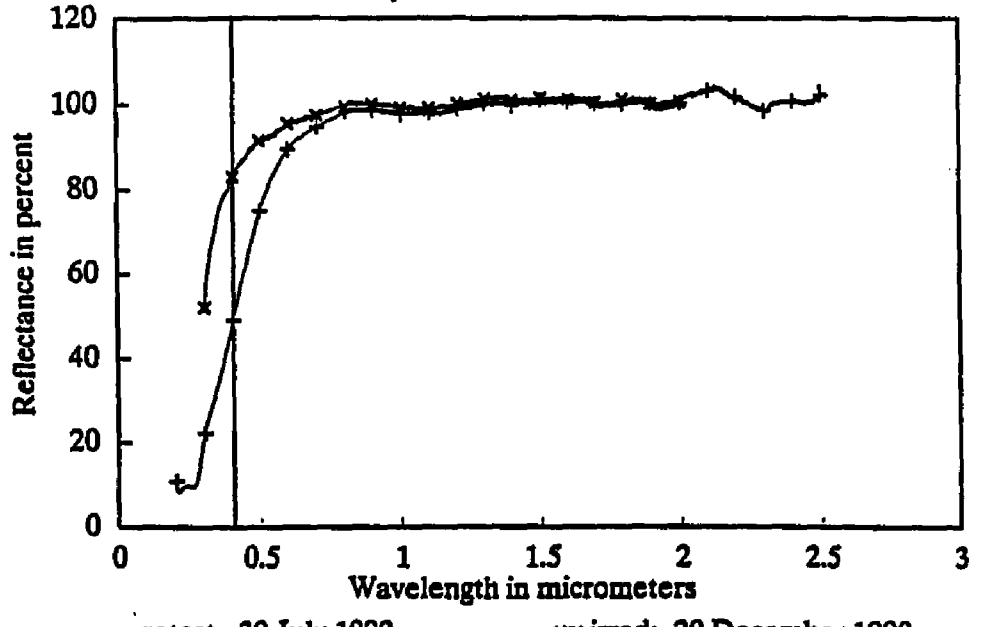

× pretest: 30 July 1990 + uv irrad: 20 December 1990

Figure 3.9. MACOR
Cary data: Reference to halon

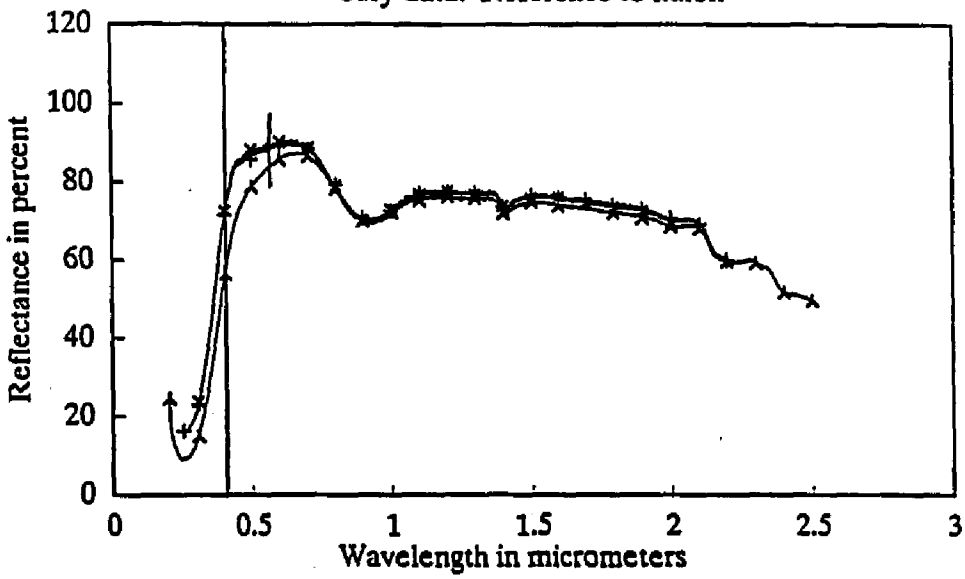

× pretest #1: 30 July 1990 + proton #2: 21 August 1990
⅄ uv irrad #1: 20 December 1990

Figure 3.10. PORCELAIN
Cary data: Reference to halon

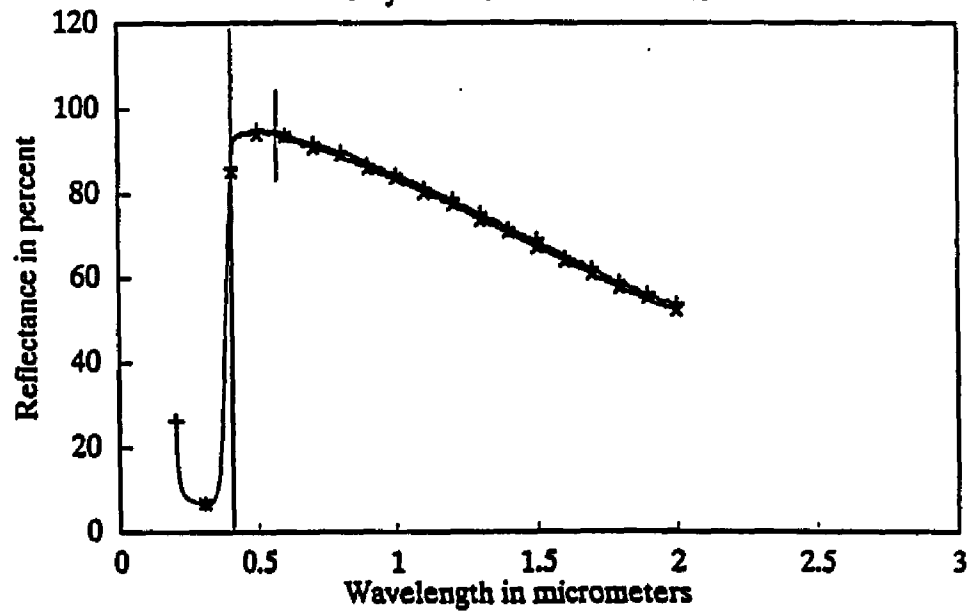

× #1 pretest: 30 July 1990 + #2 proton: 30 October 1990

Figure 3.11. PYROCERAM
Cary data: Reference to halon

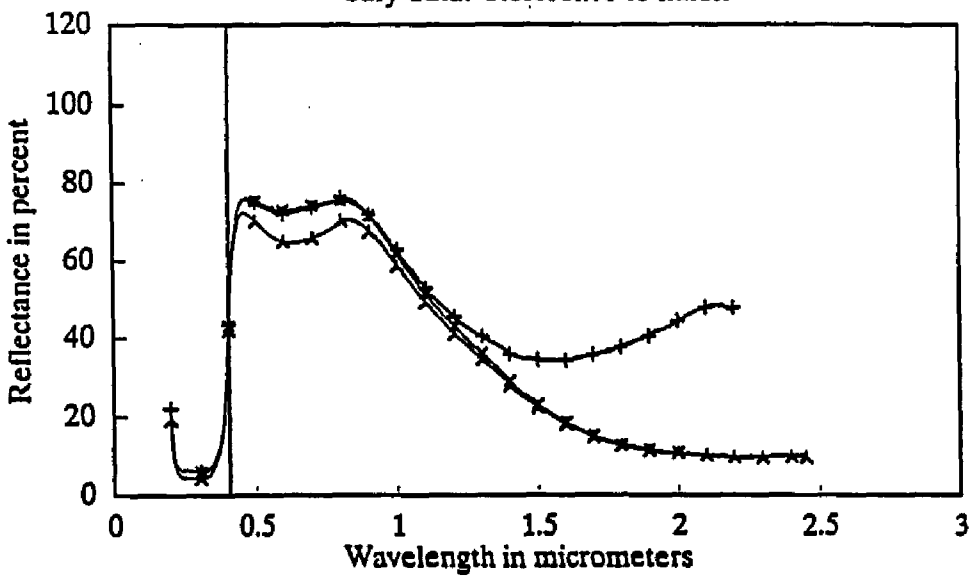

× pretest: 30 July 1990 + proton: 21 August 1990
⅄ uv irrad: 20 December 1990

Figure 3.12. SINTERED HALON
Cary data: Reference to halon

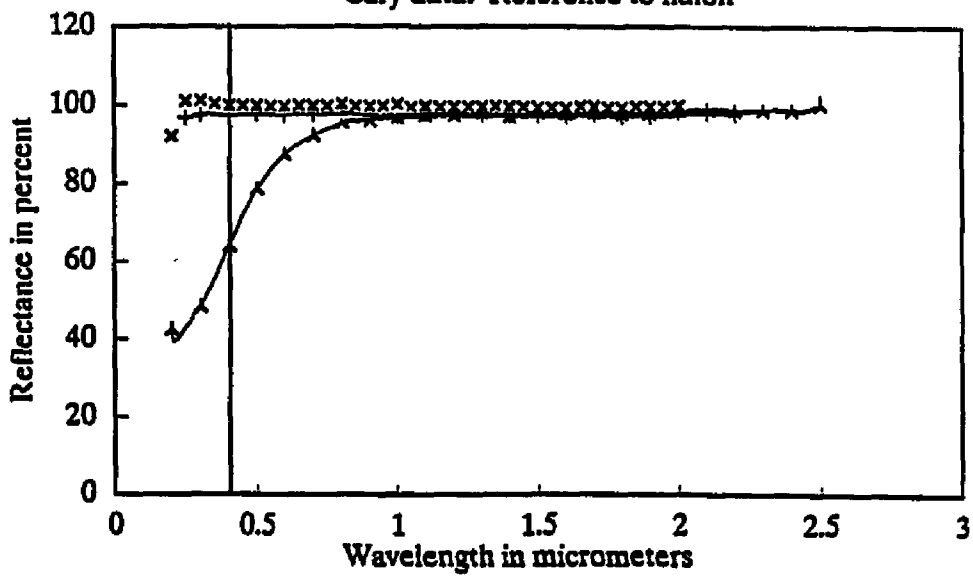

× pretest #2: 27 July 1990 + proton #2: 21 August 1990
⅄ uv irrad #1: 20 December 1990

Figure 3.13. OPTICAL-GRADE SPECTRALON
Cary data: Reference to halon

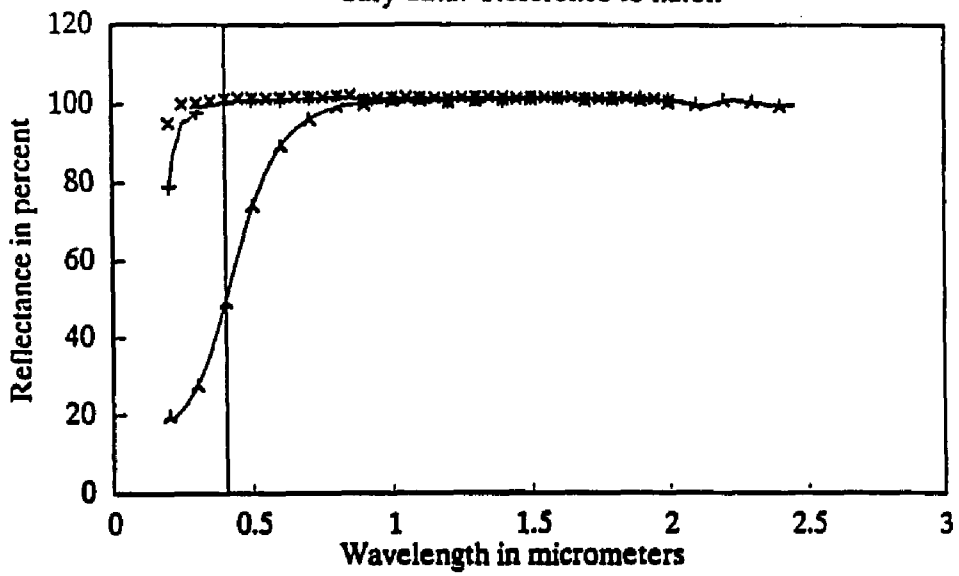

× pretest #3: 27 July 1990 + proton #3: 3 October 1990
△ uv irrad #1: 3 January 1991

Figure 3.14. LASER-GRADE SPECTRALON #7
Cary data: Reference to halon

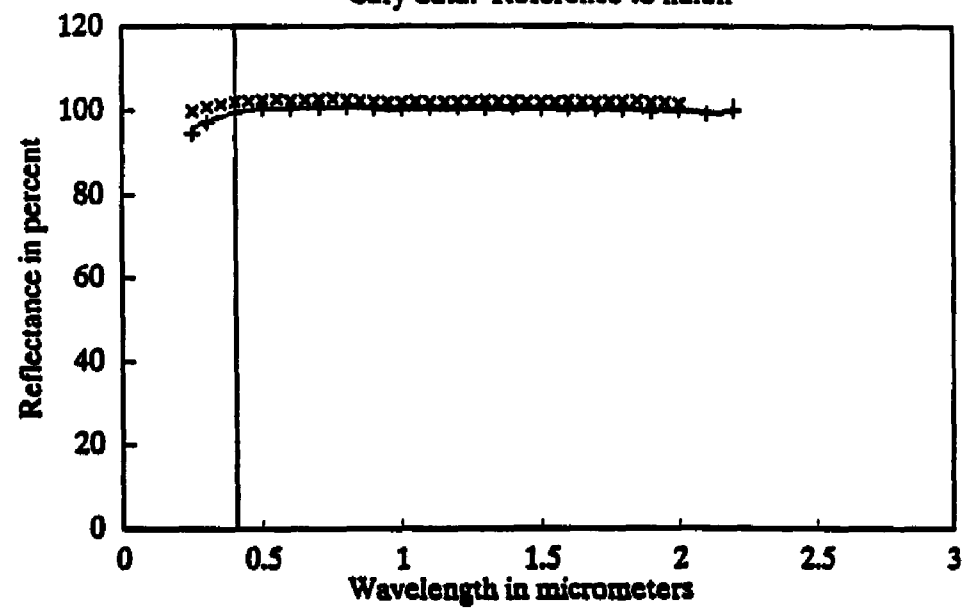

× pretest: 27 July 1990 + proton: 21 August 1990

Figure 3.15a. S13G/LO-41 #2
Cary data: Reference to halon

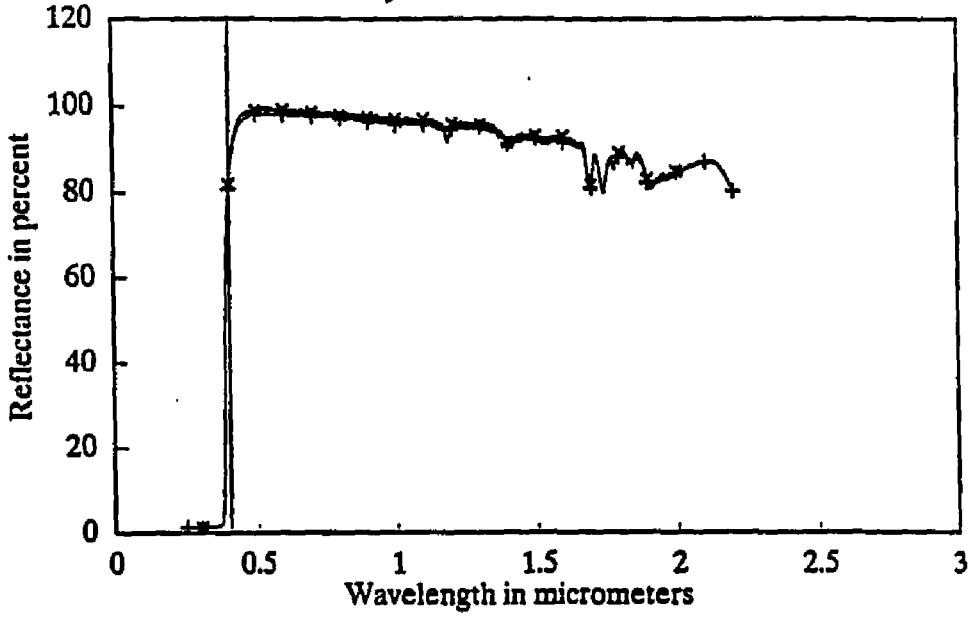

× pretest: 30 July 1990 + proton: 21 August 1990

Figure 3.15b. S13G/LO-41 #1
Cary data: Reference to halon

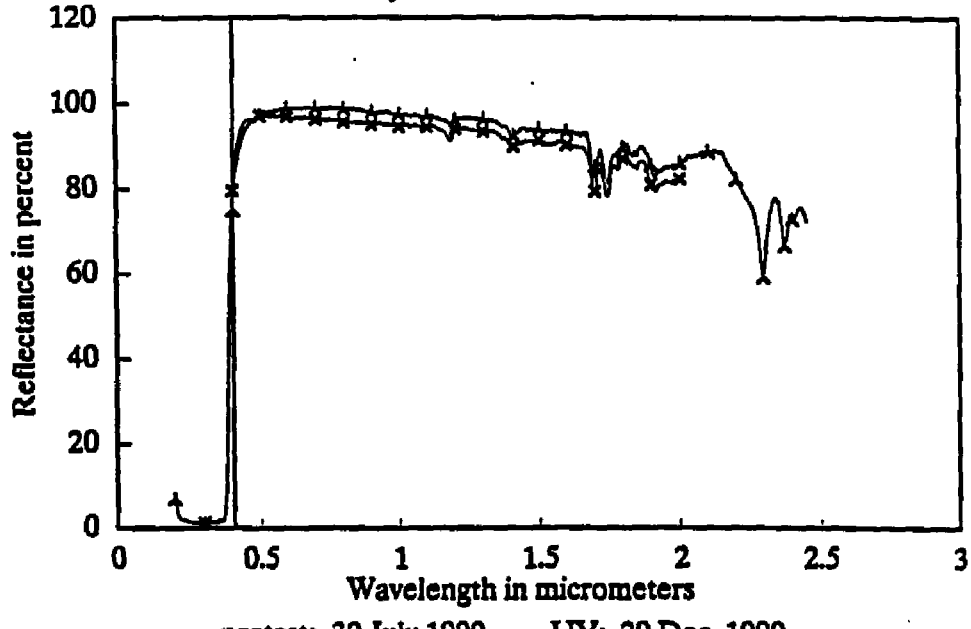

× pretest: 30 July 1990 ⅄ UV: 20 Dec. 1990

Figure 3.16a. YB-71 #1
Cary data: Reference to halon

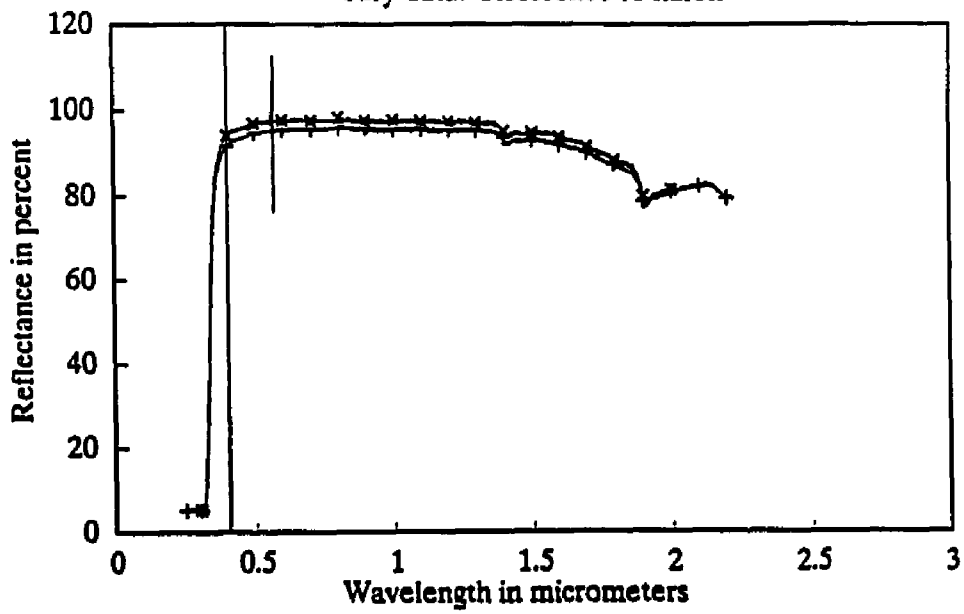

× pretest: 30 July 1990 + proton: 21 August 1990

Figure 3.16b. YB-71 #2
Cary data: Reference to halon

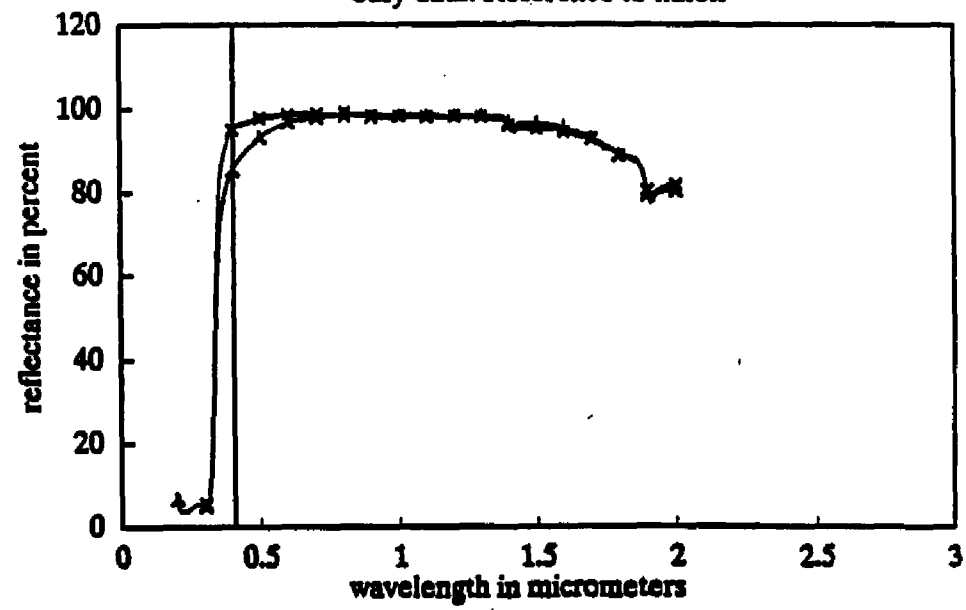

× pretest: 30 July 1990 ▲ uv irrad: 20 December 1990

Figure 3.17a. Z-93 #2
Cary data: Reference to halon

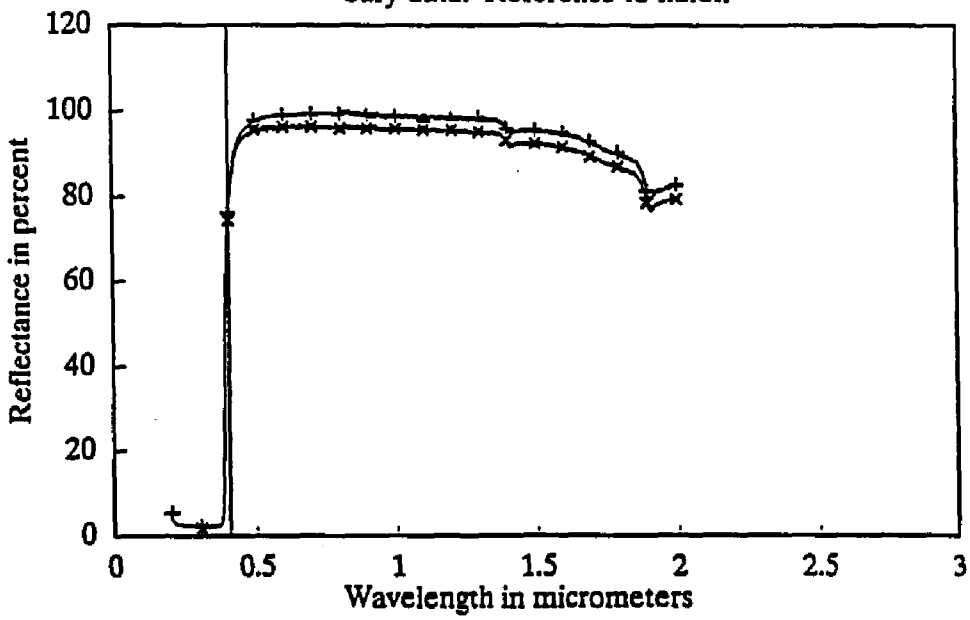

× pretest: 27 July 1990 + proton: 3 October 1990

Figure 3.17b. Z-93 #1
Cary data: Reference to halon

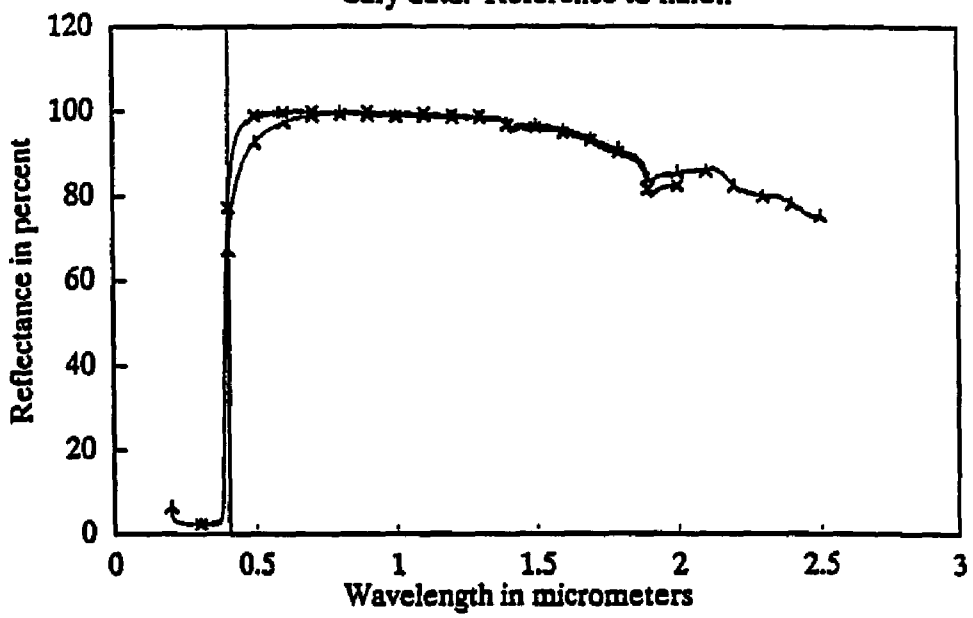

× pretest: 30 July 1990 ▲ uv irrad: 20 December 1990

Figure 3.18. PRETEST AL_2O_3 #3
BRF data: Reference to halon: 28,30 July 1990

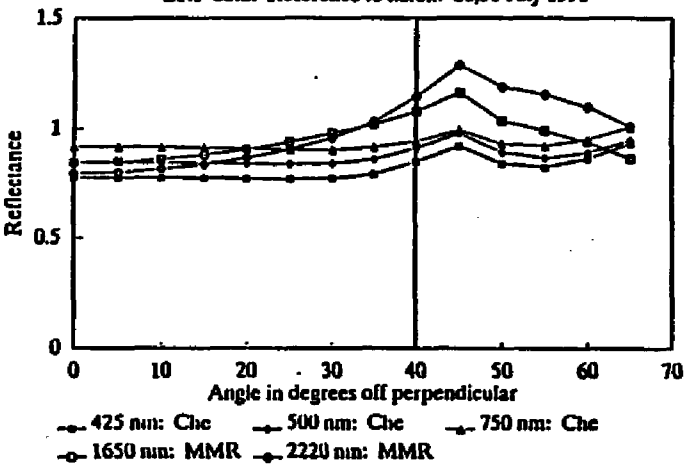

Figure 3.19. PROTON BOMBARDED AL_2O_3 #3
BRF data: Reference to halon: 5,6 September 1990

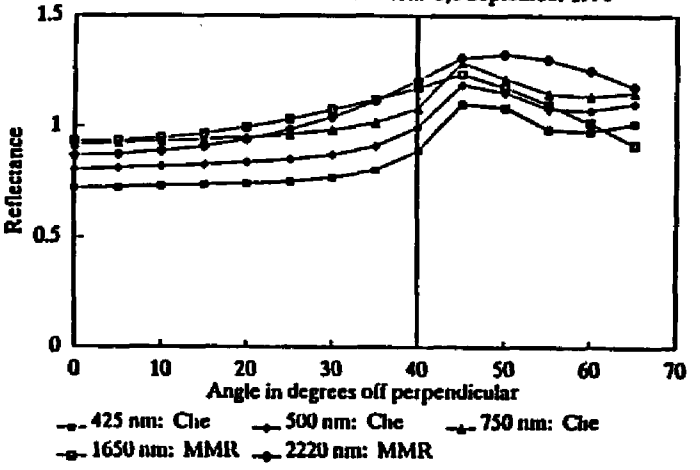

Figure 3.20. UV IRRADIATED AL_2O_3 #1
BRF data: Reference to halon: 29 December 1990

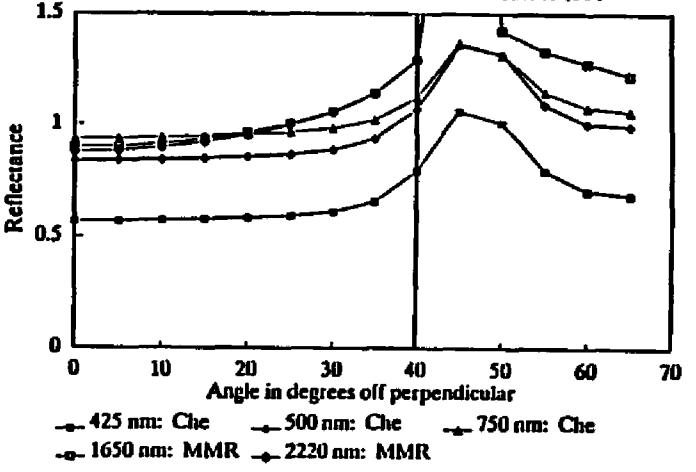

Figure 3.21. PRETEST MACOR #2
BRF data: Reference to halon: 24,28 July 1990

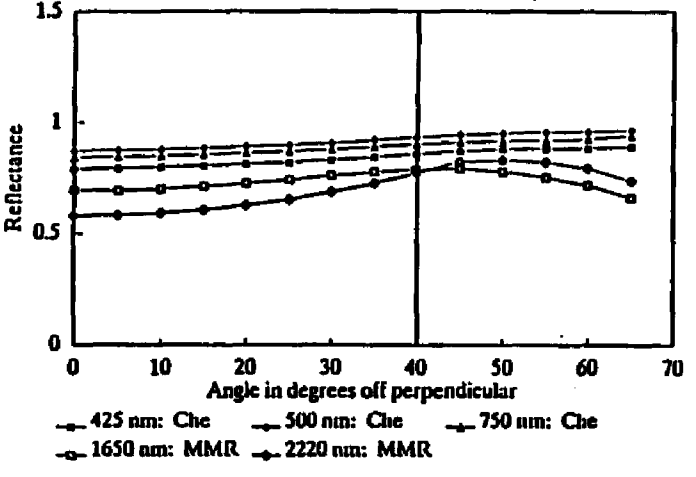

Figure 3.22. PROTON BOMBARDED MACOR #2
BRF data: Reference to halon: 5,6 September 1990

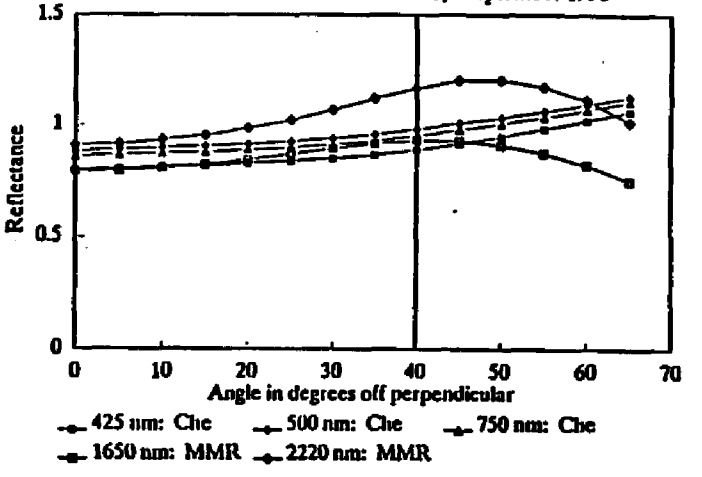

Figure 3.23. UV IRRADIATED MACOR #1
BRF data: Reference to halon: 28 December 1990

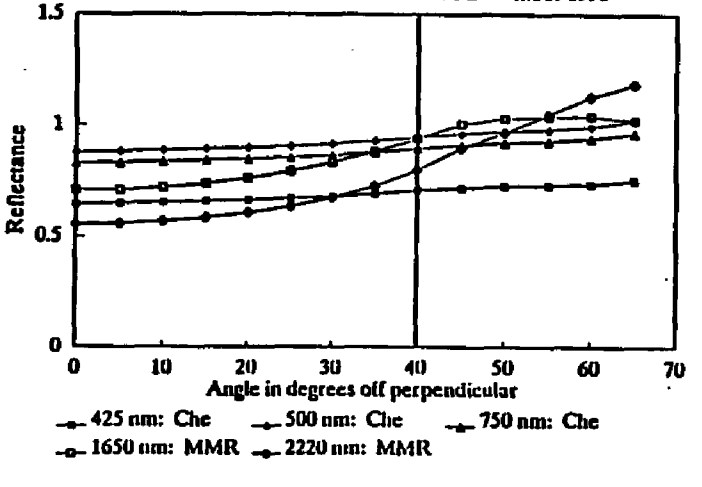

Figure 3.24. PRETEST PORCELAIN #2
BRF data: Reference to halon: 23,28 July 1990

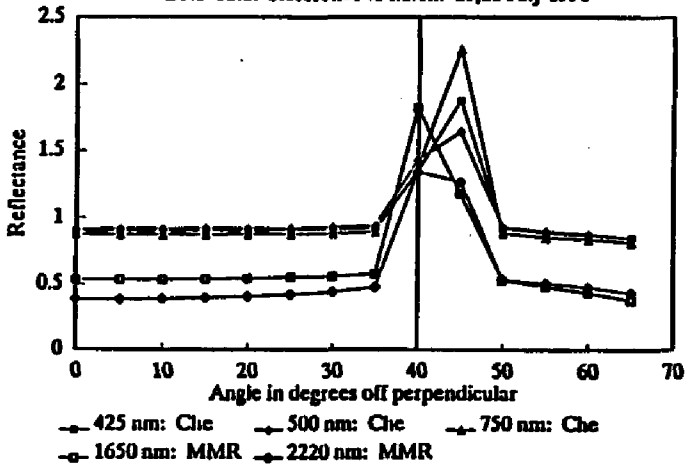

Figure 3.25. PROTON BOMBARDED PORCELAIN #2
BRF data: Reference to halon: 5,6 September 1990

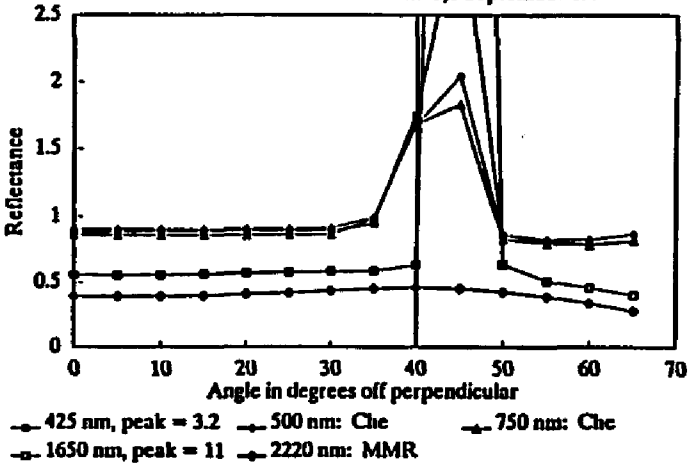

Figure 3.26. PRETEST PYROCERAM #1
BRF data: Reference to halon: 24,28 July 1990

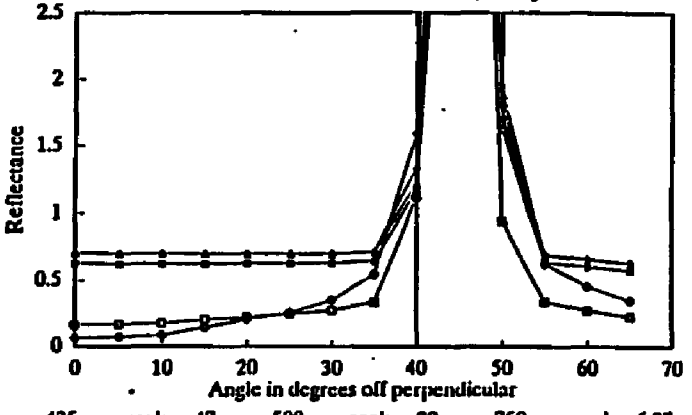

425 nm, peak = 47. 500 nm, peak = 29. 750 nm, peak =6.07
1650 nm, peak = 7. 2220 nm, peak = 7.

Figure 3.27. PROTON BOMBARDED PYROCERAM #1
BRF data: Reference to halon: 5,6 September 1990

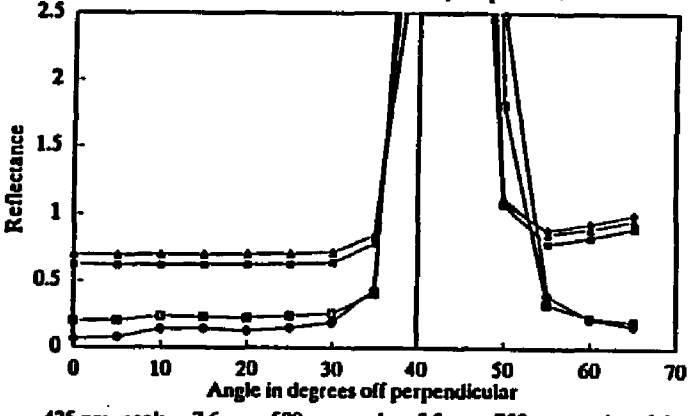

425 nm, peak = 7.6 500 nm, peak = 5.5 750 nm, peak = 6.6
1650 nm, peak = 11 2220 nm, peak = 10

Figure 3.28. UV IRRADIATED PYROCERAM #1
BRF data: Reference to halon: 28 December 1990

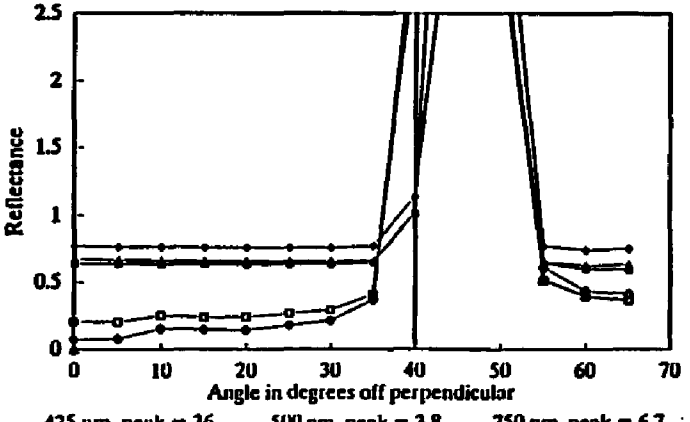

425 nm, peak = 36. 500 nm, peak = 3.8 750 nm, peak = 6.7
1650 nm, peak = 9. 2220 nm, peak = 13

Figure 3.29. PRETEST SINTERED HALON #2
BRF data: Reference to halon: 24,28 July 1990

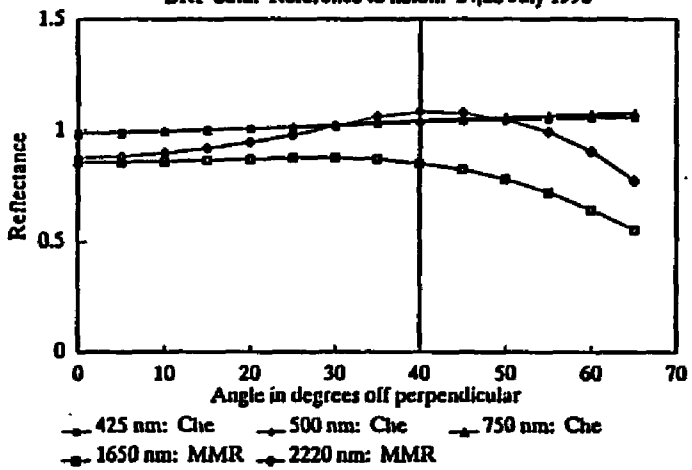

Figure 3.30. PROTON BOMBARDED SINTERED HALON #2
BRF data: Reference to halon: 5,6 September 1990

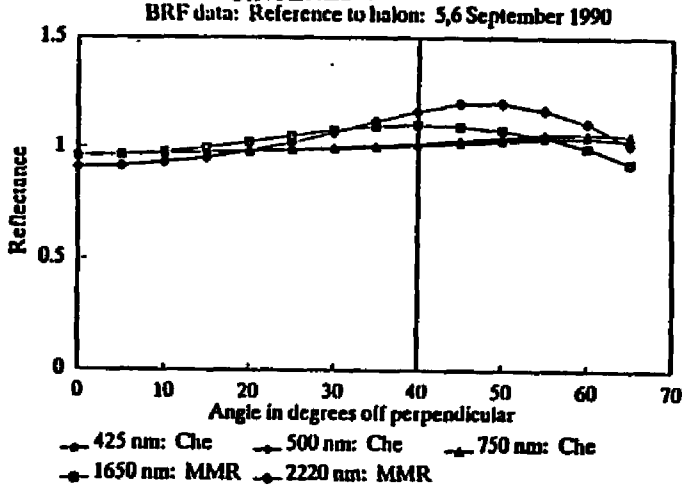

Figure 3.31. UV IRRADIATED SINTERED HALON #1
BRF data: Reference to halon: 28 December 1990

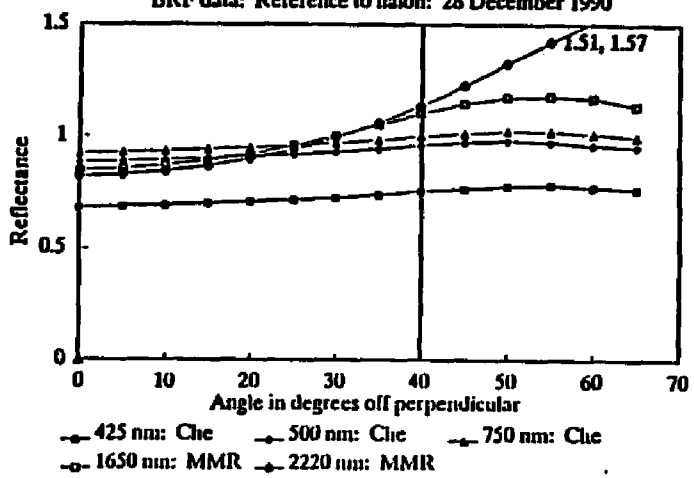

Figure 3.32. PRETEST
OPTICAL-GRADE SPECTRALON #3
BRF data: Reference to halon: 23,28 July 1990

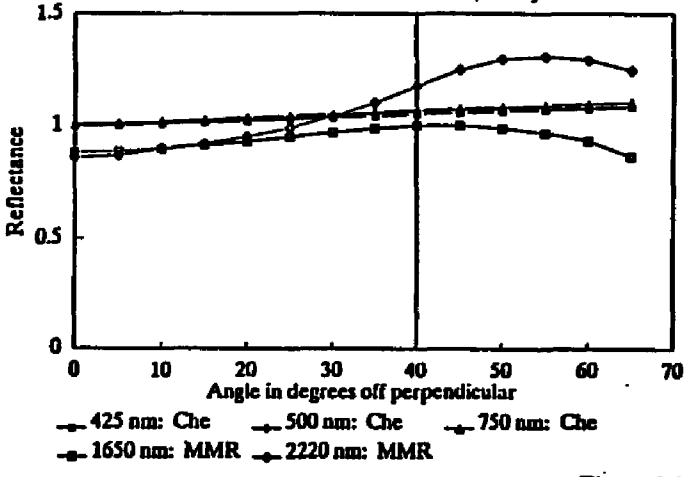

Figure 3.33. PROTON BOMBARDED
OPTICAL-GRADE SPECTRALON #3
BRF data: Reference to halon: 5,6 September 1990

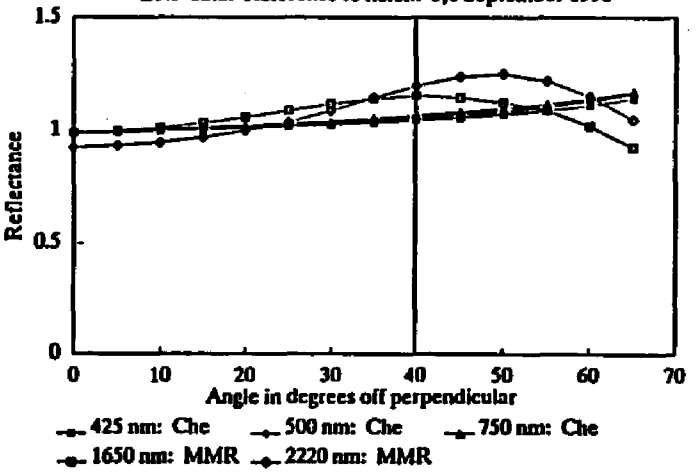

Figure 3.34. UV IRRADIATED
OPTICAL-GRADE SPECTRALON #1
BRF data: Reference to halon: 28 December 1990

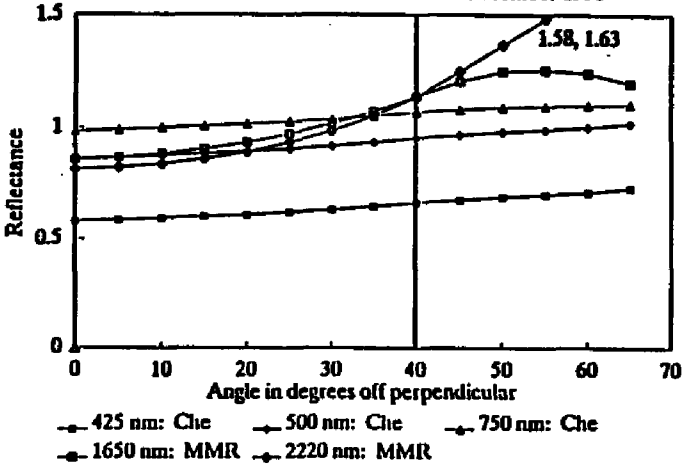

Figure 3.35. PRETEST
LASER-GRADE SPECTRALON #7
BRF data: Reference to halon: 23,28 July 1990

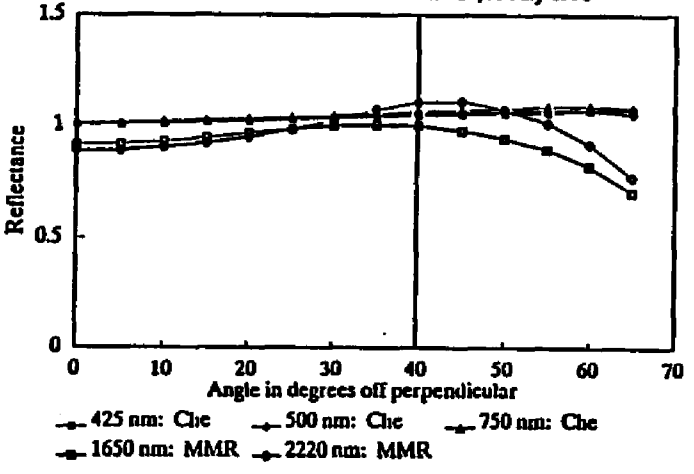

Figure 3.36. PROTON BOMBARDED
LASER-GRADE SPECTRALON #7
BRF data: Reference to halon: 5,6 September 1990

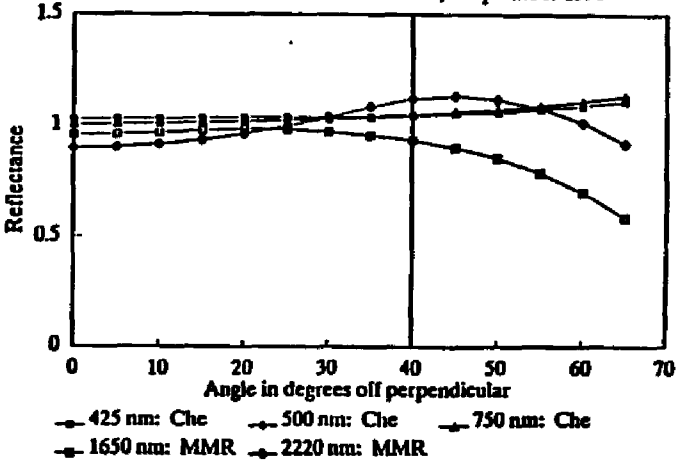

Figure 3.37. PRETEST S13G/LO-41 #2
BRF data: Reference to halon: 24,28 July 1990

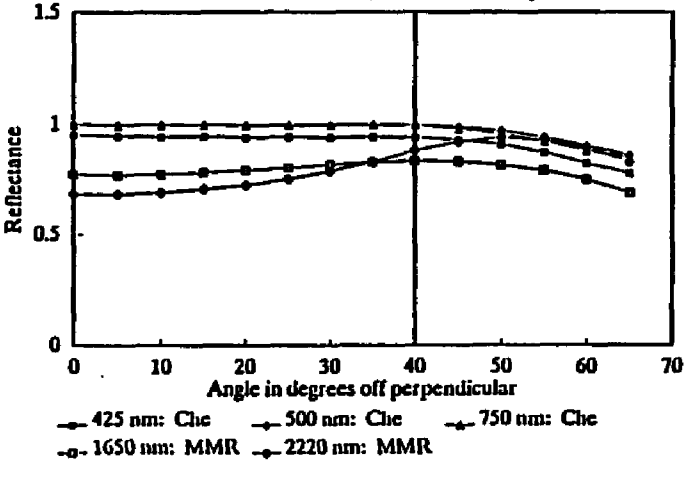

Figure 3.38. PROTON BOMBARDED S13G/LO-41 #2
BRF data: Reference to halon: 5,6 September 1990

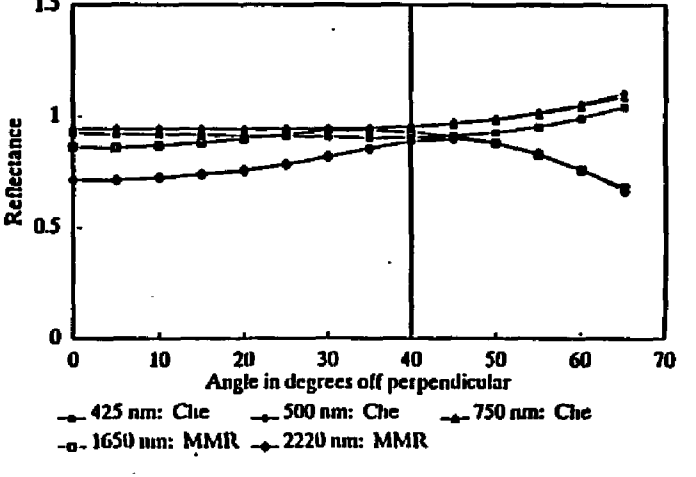

Figure 3.39. PRETEST YB-71 #1
BRF data: Reference to halon: 23,28 July 1990

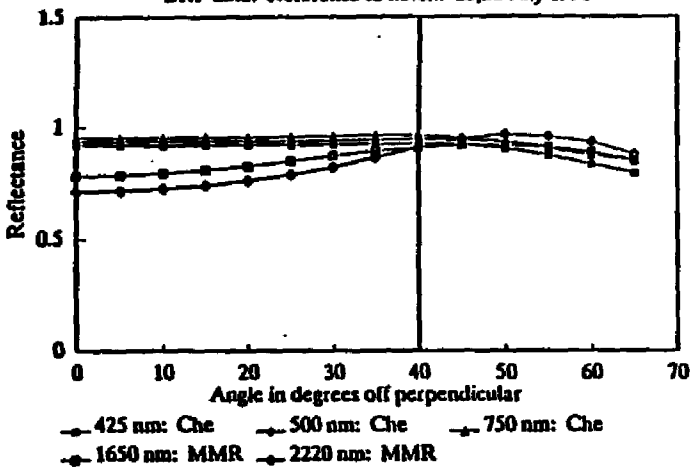

Figure 3.40. PROTON BOMBARDED YB-71 #1
BRF data: Reference to halon: 5,6 September 1990

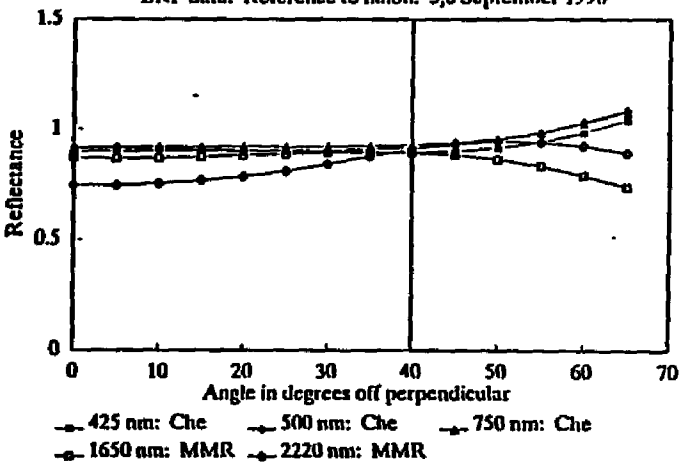

Figure 3.41. UV IRRADIATED YB-71 #2
BRF data: Reference to halon: 28 December 1990

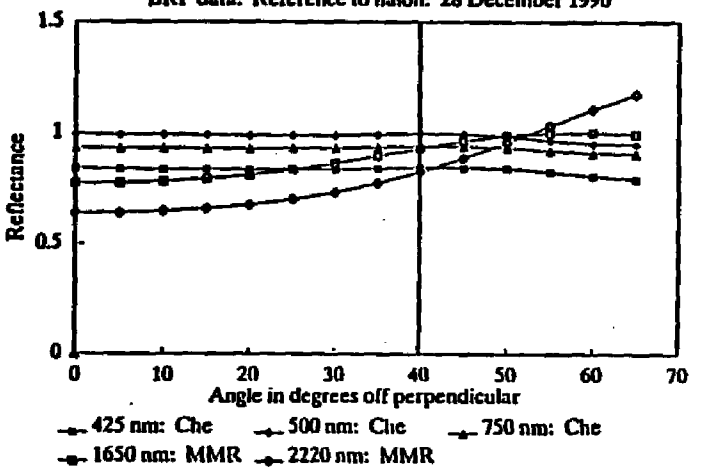

Figure 3.42. PRETEST Z-93 #2
BRF data: Reference to halon: 23,28 July 1990

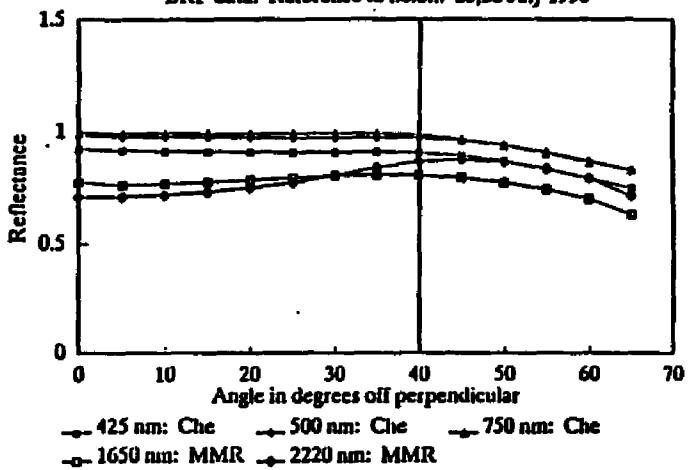

Figure 3.43. PROTON BOMBARDED Z-93 #2
BRF data: Reference to halon: 5,6 September 1990

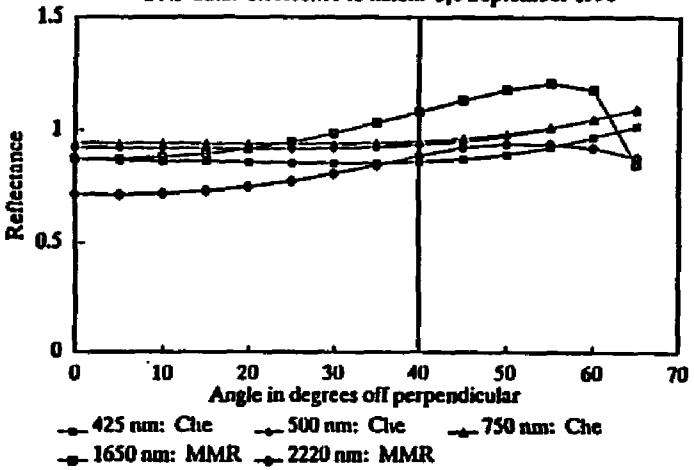

Figure 3.44. UV IRRADIATED Z-93 #1
BRF data: Reference to halon: 28 December 1990

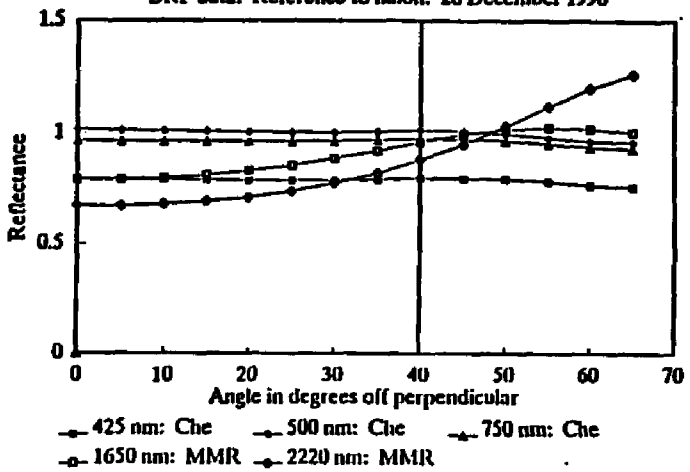

Figure 3.45. Al_2O_3 DEGREE-OF-POLARIZATION
Reference to halon; 19 Dec. 1990 (proton); 21 Nov. 1990 (UV)

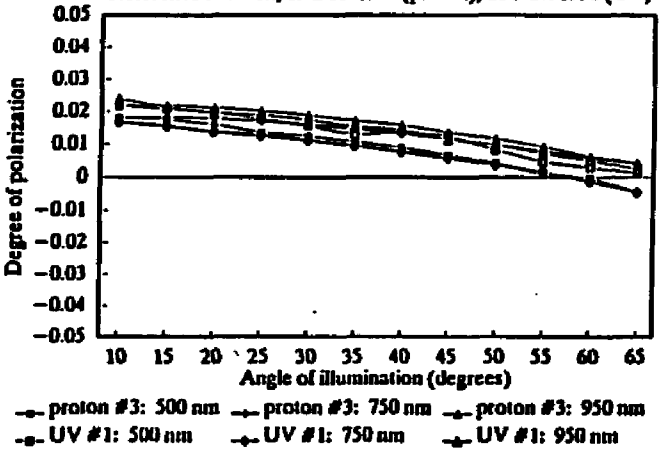

Figure 3.46. Al_2O_3 DEGREE-OF-DEPOLARIZATION
Reference to halon; 21 Dec. 1990

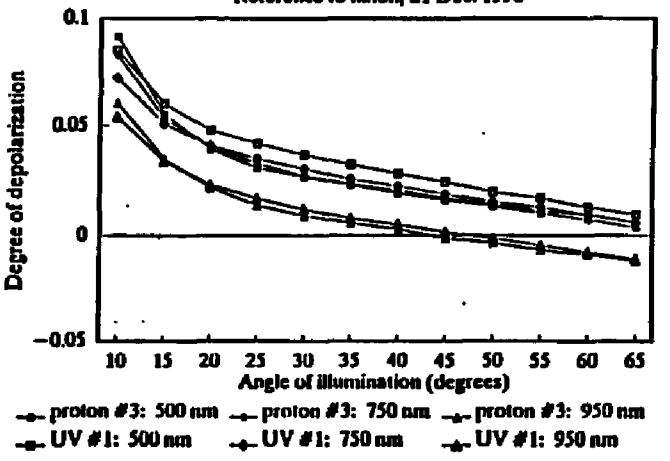

Figure 3.47. MACOR DEGREE-OF-POLARIZATION
Reference to halon; 19 Dec. 1990 (proton); 21 Nov. 1990 (UV)

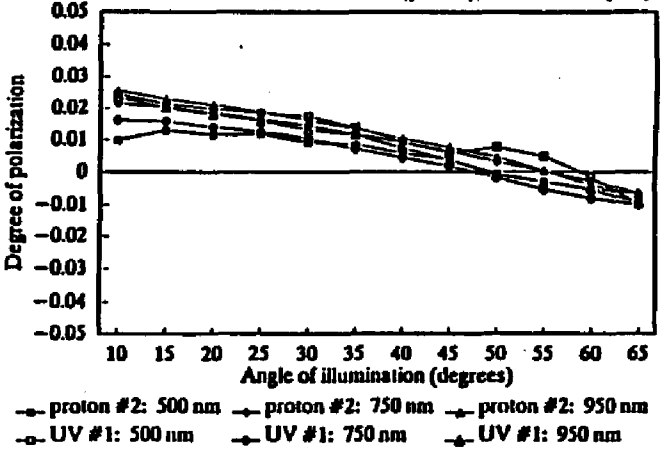

Figure 3.48. MACOR DEGREE-OF-DEPOLARIZATION
Reference to halon; 21 Dec. 1990

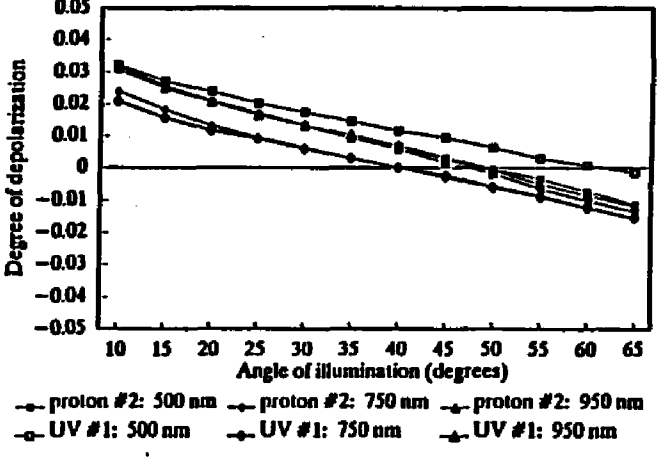

Figure 3.49. PORCELAIN
DEGREE-OF-POLARIZATION
Reference to halon; 19 Dec. 1990

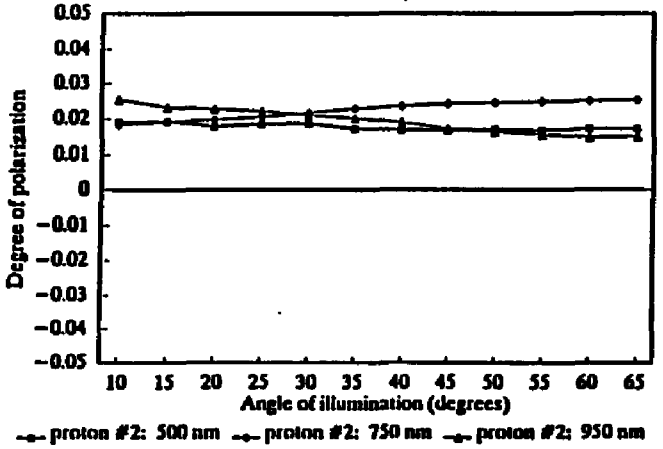

Figure 3.50. PORCELAIN
DEGREE-OF-DEPOLARIZATION
Reference to halon; 21 Dec. 1990

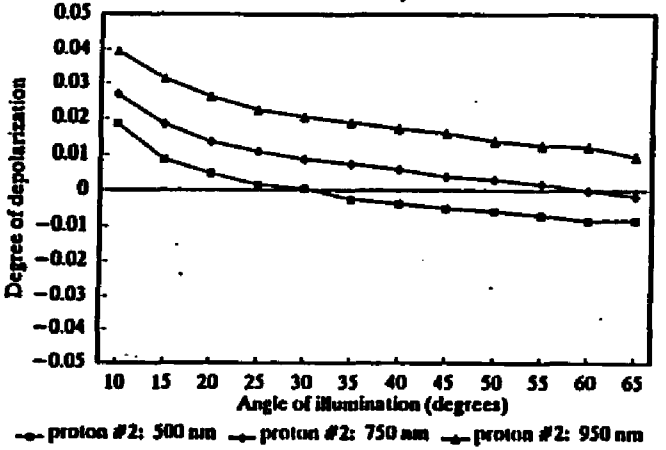

Figure 3.51. PYROCERAM
DEGREE-OF-POLARIZATION
Reference to halon; 19 Dec. 1990 (proton); 21 Nov. 1990 (UV)

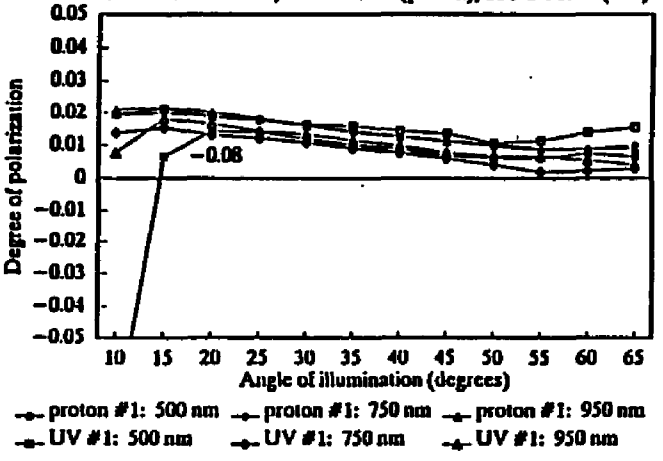

Figure 3.52. PYROCERAM
DEGREE-OF-DEPOLARIZATION
Reference to halon; 21 Dec. 1990

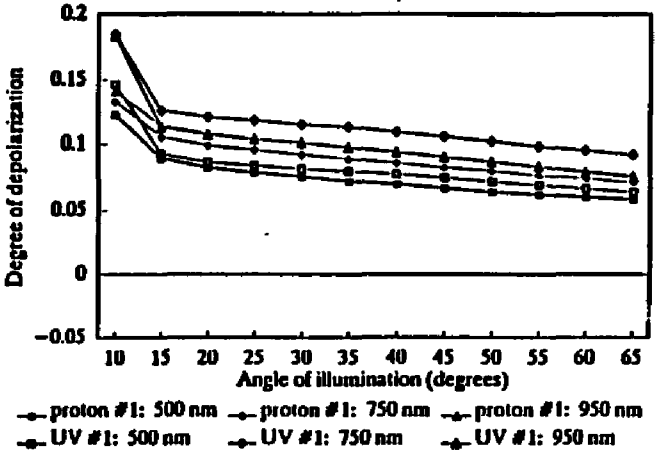

Figure 3.53. SINTERED HALON
DEGREE-OF-POLARIZATION
Reference to halon; 19 Dec. 1990 (proton); 21 Nov. 1990 (UV)

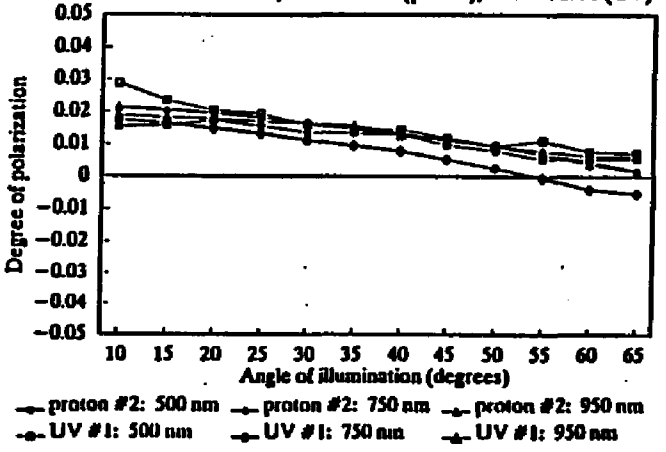

Figure 3.54. SINTERED HALON
DEGREE-OF-DEPOLARIZATION
Reference to halon; 21 Dec. 1990

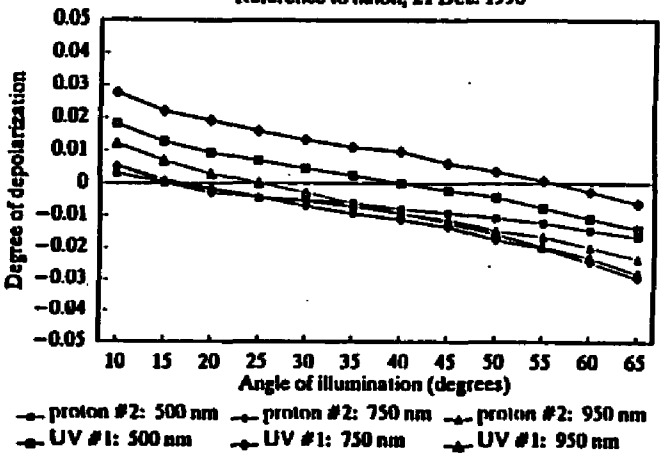

Figure 3.55. OPTICAL-GRADE SPECTRALON
DEGREE-OF-POLARIZATION
Reference to halon; 19 Dec.1990 (proton); 4 Jan. 1990 (UV)

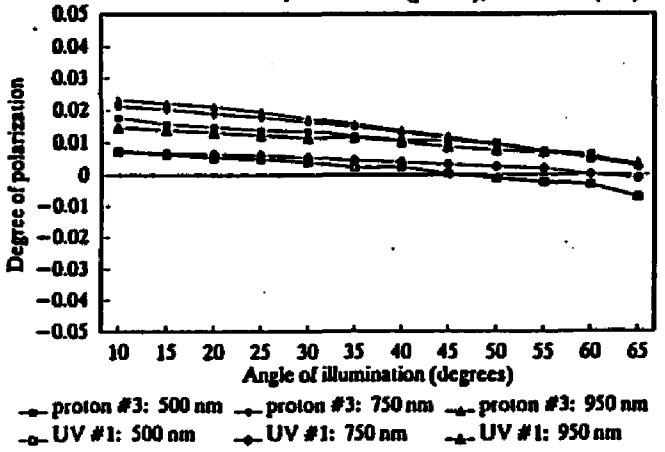

Figure 3.56. OPTICAL-GRADE SPECTRALON
DEGREE-OF-DEPOLARIZATION
Reference to halon; 21 Dec. 1990

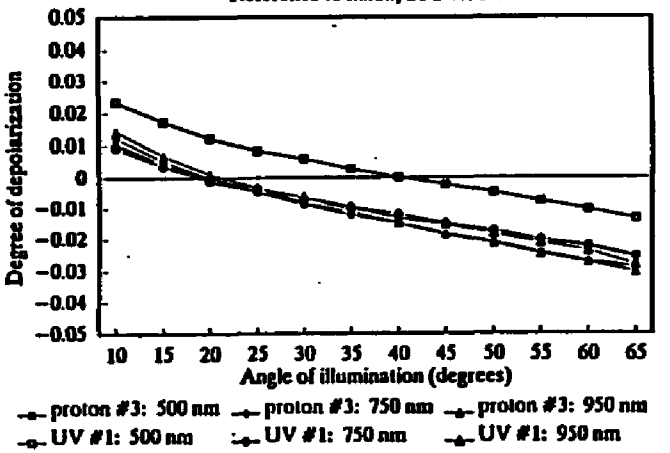

Figure 3.57. LASER-GRADE SPECTRALON DEGREE-OF-POLARIZATION
Reference to halon; 19 Dec. 1990

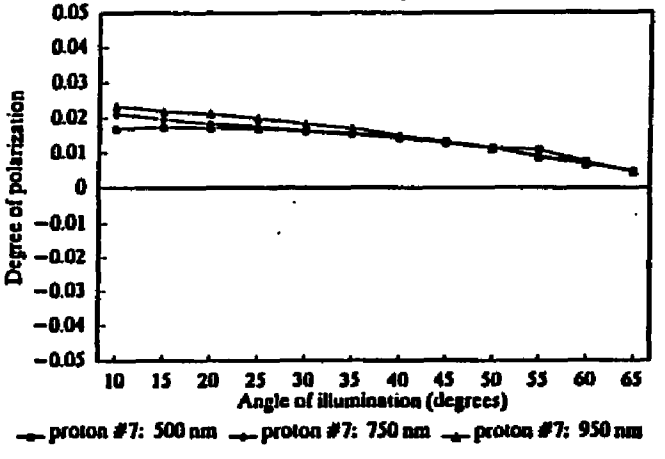

Figure 3.58. LASER-GRADE SPECTRALON DEGREE-OF-DEPOLARIZATION
Reference to halon; 21 Dec. 1990

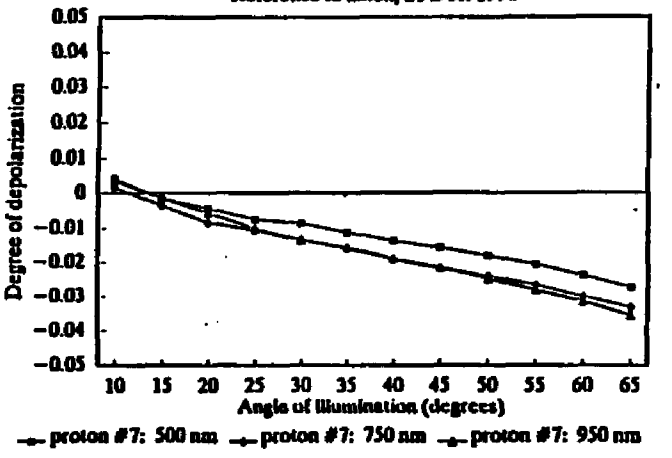

Figure 3.59. S13G/LO-41 DEGREE-OF-POLARIZATION
Reference to halon; 19 Dec. 1990

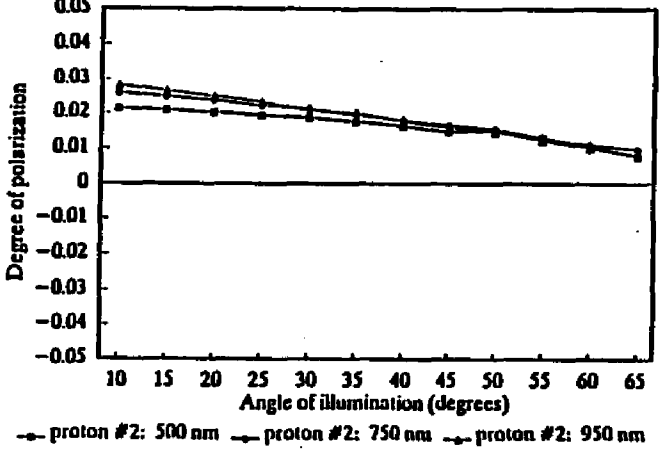

Figure 3.60. S13G/LO-41 DEGREE-OF-DEPOLARIZATION
Reference to halon; 21 Dec. 1990

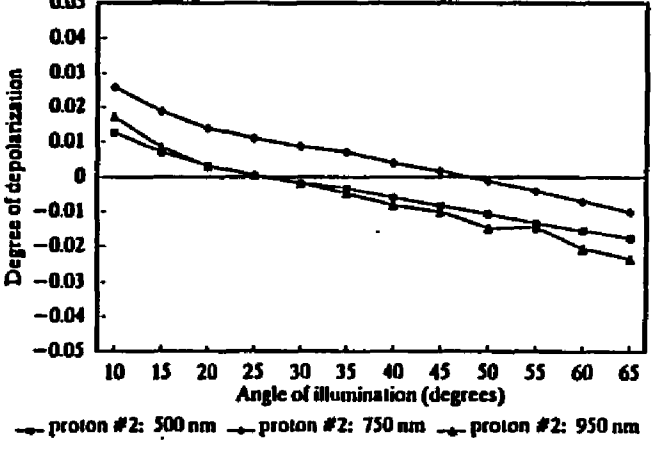

Figure 3.61. YB-71 DEGREE-OF-POLARIZATION
Reference to halon; 19 Dec. 1990 (proton); 4 Jan. 1990 (UV)

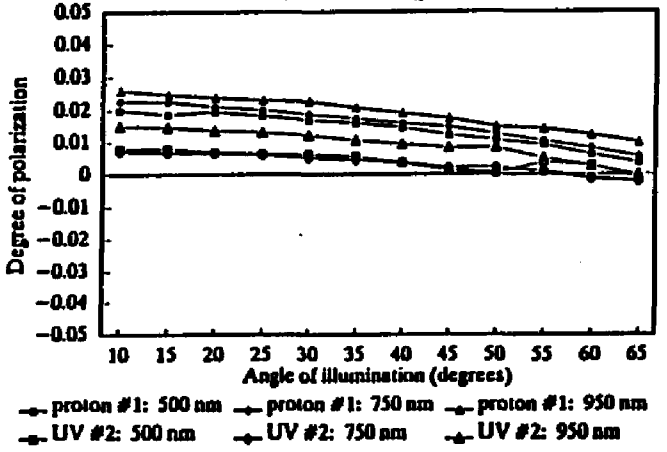

Figure 3.62. YB-71 DEGREE-OF-DEPOLARIZATION
Reference to halon; 21 Dec. 1990

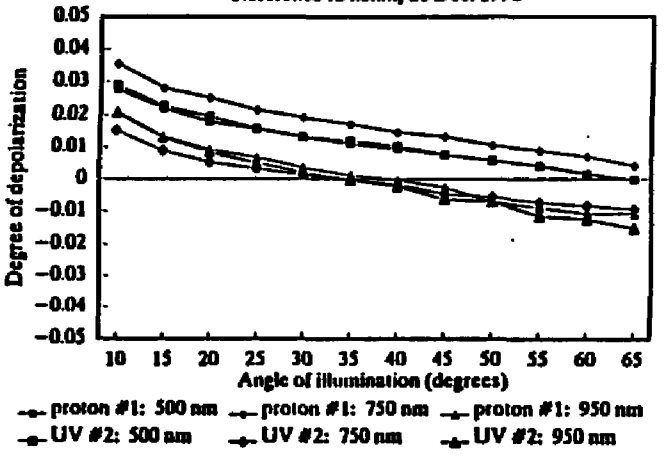

Figure 3.63. Z-93 DEGREE-OF-POLARIZATION
Reference to halon; 19 Dec. 1990 (proton); 21 Nov. 1990 (UV)

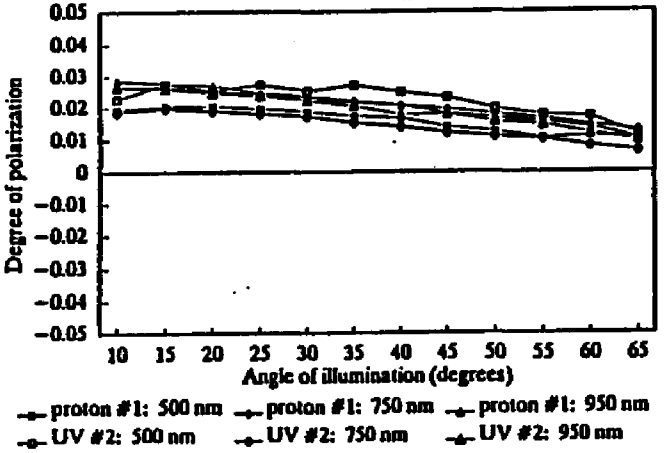

Figure 3.64. Z-93 DEGREE-OF-DEPOLARIZATION
Reference to halon; 21 Dec. 1990

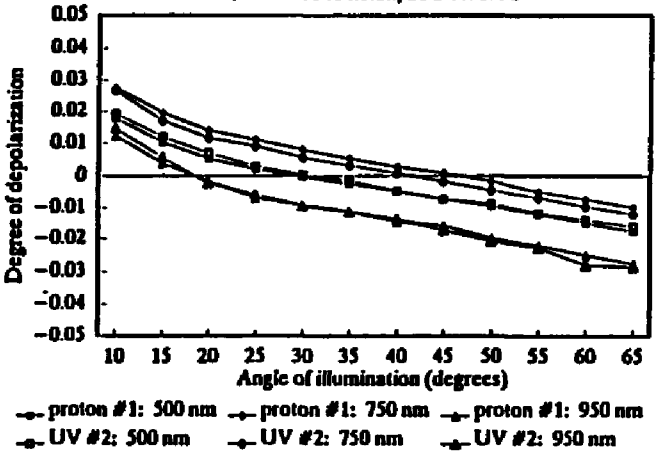

Table 3.2 lists the results from the different tests. Of the ceramics, Al_2O_3 and Macor are the best materials even though they both have brown tints after UV irradiation. Both Pyroceram and Porcelain have a large specular component which had an average width of 15°. Depending on the geometry, this may or may not be a desirable characteristic for a solar diffuser.

The PTFE compounds exhibited marked decreases (20-40%) in reflectance after UV irradiation. They also luminesced with a strong purple color.

The IITRI paints exhibited the least change in reflectance after UV irradiation. Z-93 luminesced a strong yellow color and therefore may not be suitable as a solar diffuser. Of the UV irradiated samples, YB-71 fared the best with the least overall change. The paint S13G/LO-41 had spectral structure beyond 2.0 μm which may be hard to monitor.

Table 3.2. Candidate material test results

SAMPLE	PRETEST				AFTER PROTON BOMBARDMENT			AFTER UV IRRADIATION				
	Luminescence	Specular BRF	Diffuse R	BRF	Change in diffuse R	Change in BRF	% Degree of depolar.	Color	Change in diffuse R	% Diffuse R at 0.4μm	Change in BRF	Change in degree of depolar.
Al_2O_3	no	yes	approx. 100%	BRF greater than 75%	almost no change	specular BRF increase	10	brown	decrease below 0.7 μm	40	decrease, 27% at 425 nm, specular increase	decrease 11%
Macor	no	no	falls off in SWIR		almost no change	increase in SWIR	3.2	brown	decrease below 0.7 μm	12	decrease, 18% at 425 nm	almost no change
Porcelain	no	yes strong	decrease linearly with increasing λ		almost no change	almost no change, no specular at 2220 nm	1.9 to 3.9	NOT TESTED				
Pyroceram	no	yes very strong	max. 76%, less than 20% above 1.5 μm		unexplained increase in SWIR	almost no change	14	blue-gray	decrease max. 12% at 0.6 μm	5	increase, max. 39% at 750 nm	increase, max. 39% at 750 nm

* Degree of polarization was less than 3% for all samples.

Table 3.2. Candidate material test results, cont.

SAMPLE	PRETEST				AFTER PROTON BOMBARDMENT			AFTER UV IRRADIATION				
	Luminescence	Specular BRF	Diffuse R	BRF	Change in diffuse R	Change in diffuse R	% Degree of depolar.	Color	Change in BRF	% Diffuse R at 0.4 μm	Change in BRF	Change in degree of depolar.
Sintered Halon	yes purple	no	approx. 100%	flat BRF	almost no change	increase in SWIR	0.6	brown	decrease	36	decrease, 31% at 425 nm	increase, greater than 100%
Spectralon (optical)	yes purple	no	approx. 100%	flat BRF	almost no change	increase in SWIR	1.2	brown	decrease	51	decrease, 41% at 425 nm	increase, 150% at 500 nm
Spectralon (laser)	yes purple	no	approx. 100%	flat BRF	almost no change	almost no change	0.4	NOT TESTED				
S13G/LO-41	no	no	structure in SWIR	flat BRF	almost no change	almost no change except increase at 1650 nm	1.3 to 2.6	no change, sample appeared dirty	more pronounced structure in SWIR	1.5	NOT TESTED	
YB-71	no	no	sharp change at 1.9 μm	flat BRF	slight decrease	almost no change	2.1 to 3.5	brown tint	decrease	10	decrease in SWIR	decrease, 57% at 750 nm
Z-93	yes yellow	no	sharp change at 1.9 μm	flat BRF	slight increase	almost no change except increase at 1650 nm	1.2	tan	decrease below 0.6 μm	13	almost no change except decrease at 425 nm	almost no change

* Degree of polarization was less than 3% for all samples.

CHAPTER IV

CONCLUSIONS

The first half of this thesis has demonstrated that a simple radiometer with a solar diffuser panel is feasible for calibrating multispectral satellite sensors and that a satisfactory ratio of signal levels for ease in instrument characterization is readily achievable. Furthermore, it has been shown that the FOV can be selected and controlled as desired. The second half of this thesis discussed the spectral reflectance, directional and polarization properties and stability with time, and environmental influences on selected materials. The tested materials consisted of ceramic materials, different types of sintered halon and white paints, which preliminary tests had proven to be near-lambertian.

An analysis shows that the estimated uncertainty in the calibration method with respect to the sun is two percent or less depending on the general stray light problem, which is the dominant uncertainty. Therefore, a detailed design of the RR and panel system needs to consider the reduction of stray radiation to less than 1%, while also considering the linearity and dynamic range of the RR detectors, the stability of all optical and mechanical elements in the space environment, and the refractive/reflective alternatives. The design must minimize the effect of contamination on the surface(s) of the field lens(es) inside the RR. If the field lens is located near the focus of the objective lens, the contamination may effect the ratio. This effect became evident with the test radiometer that had a chip in the field lens which caused a slight shadow on the detector when looking at the lamp.

Along with the design, the number and location of spectral channels needs to be determined to adequately cover the reflected solar region. Enough channels must be chosen to ensure that broad spectral reflectance changes in the panel are detected. The channel bandpasses must be wide enough for sufficient spectral coverage.

The entire mounting scheme for the radiometer and panel on the spacecraft needs to be carefully studied, particularly with respect to all direct and reflected sources that irradiate the panel or enter the field of view of the radiometer. For example, the directional radiance of the surface of the platform core needs to be known to determine how it will influence the irradiance of the panel (in particular -- will it cause specular components to be seen by the sensors?). Simple means to minimize extraneous radiation incident on the panel should be studied.

Since the panel radiance is proportional to the cosine of the solar incidence angle, the geometry of the diffuser panel with respect to the sun is critical, particularly for angles greater than 30° from normal. (As mentioned in Section 2.3 of this thesis, the accuracy with which the angle of incidence on the panel needs to be known is only critical in the no-stray-light case.) In addition, the greater the angle of incidence of the solar radiation on the panel the more important it is to know the BRDF of the panel and its stability with exposure to sunlight and contaminants. It is desirable to have the view angle of the RR close to that of the multispectral satellite sensor.

The panel material tests described in this paper should be considered preliminary rather than rigorous. For example, in the handling of the samples, which is critical in terms of contamination, no one person was responsible for accompanying the samples throughout the tests and measurements, although every effort was made to package and handle them carefully. The results listed in Table 3.2 do indicate that several materials, such as Pyroceram and Porcelain, are not worth testing again. A second round of tests should include a better Al_2O_3, a PTFE material with lower contamination, and YB-71. Additional consideration should be given to the thermal and mechanical properties of the materials.

Bruegge et al. (1991) have discussed the possibility that contaminants in the PTFE powder may be the cause of their luminescence and decreased reflectance in the blue following UV irradiation. The preliminary results described here deserve further study and the tests should be repeated for the PTFE compounds if they can be produced with lower contaminant levels and do not exhibit a tendency to attract contaminants. The wavelength(s) which excited the PTFE compounds should be determined in order to arrive at an estimate of how much the luminescence will affect the radiance of the panel. If these contaminant problems can not be solved, and the rapid deterioration of the reflectance of PTFE compounds in the blue is verified, they would probably not be the first choice for the solar panels proposed for HIRIS, MODIS-N and -T, and in particular for the solar-illuminated integrating spheres proposed for use on MODIS-T. The optical properties of IITRI paint YB-71 after proton exposure and UV irradiation appear, from the results of this study, to be superior to those of the PTFE compounds for the above sensors.

It is interesting to note that Harada (1991), after visually inspecting a sample of YB-71 from the Long Duration Exposure Facility states that the sample exhibited no apparent color change, cracks, chips or signs of peeling after about six years in low earth orbit.

REFERENCES

Barnes Engineering Company, "Operations and service instructions", pp. 1-1 to 1-3 and 3-1 to 3-3.

Begni, G., M. C. Dinguirard, R. D. Jackson, and P. N. Slater, "Absolute calibration of the SPOT-1 HRV cameras", SPIE 660:66-76 -- *Earth Remote Sensing Using the Landsat Thematic mapper and SPOT Sensor Systems, (1986).*

Bruegge, C. J., A. E. Stiegman, D. R. Coulter, R. R. Hale, D. J. Diner and A. W. Springsteen, "Reflectance stability analysis on Spectralon diffuse calibration panels", SPIE 1493:in press, Orlando, Florida, (1991).

Budde, W., "Large-flux-ratio linearity measurements on Si photodiodes", *Applied Optics*, 21:3699-1701, (15 October 1982).

Che, N., R. D. Jackson, A. L. Phillips, and P. N. Slater, "The use of field radiometers in reflectance factor and atmospheric measurements", SPIE 499:24-33, San Diego, California, (1984).

Chen, T., "Optical sensor contamination study", Boeing Aerospace Company, RADC-TR-86-232, (1987).

Corning Glass Works, "Material information", Code: 9617, Corning, New York, (1980).

Engel, J. L. , and O. Weinstein, "The Thematic Mapper - An overview", IEEE IGARSS '82, Digest Vol. I, WP-1:1, (1982).

Gilmore, M. R., "Ultraviolet degradation of nine samples for the Jet Propulsion Laboratory", TRW Final Report L123.16g-90-47, (1990).

Harada, Y., IITRI, personal communication, (April 1991).

Harada, Y., R. J. Mell, and D. R. Wilkes, "The effect of the space environment on thermal control coatings", SPIE 1330:in press, San Diego, California, (1990).

Harada, Y., and R.J. Mell, "Inorganic thermal control coatings: A review", AIAA 21st Aerospace Sciences Meeting, Paper no. AIAA-83-0074, Reno, Nevada, (1983).

Hunton, D. E., "Shuttle glow", *Scientific American*, 92-98, (November 1989).

Labsphere, Inc., "Reflectance technologies: Price and ordering guide", North Sutton, NJ, (1990).

Lean, J., "Contribution of ultraviolet irradiance variations to changes in the sun's total irradiance", *Science*, 244:197-200, (1989).

Palmer, J. M., "Stray light effects on calibration using a solar diffuser", SPIE 1493:in press, Orlando, Florida, (1991).

REFERENCES, CONTINUED

Palmer, J. M., and P. N. Slater, "Ratioing radiometer for use with a solar diffuser", SPIE 1493:in press, Orlando, Florida, (1991).

Slater, P. N., S. F. Biggar, R. G. Holm, R. D. Jackson, Y. Mao, M. S. Moran, J. M. Palmer and B. Yuan, "Reflectance- and radiance-based methods for the in-flight absolute calibration of multispectral sensors", *Remote Sensing of Environment*, 22:11-37, (1987).

Springsteen, A. W., Labshpere, Personal communication, (April 1991).

Willson, R. C., and H. S. Hudson, "Solar luminosity variations in solar cycle 21", *Nature*, No. 6167, 332:810-812, (1988).

Varian Instrumentation, "Accessories for Cary UV-visible spectrometer -- Operations manual", Report no. 183-188, (1990).